

Three-body scattering at intermediate energiesH. Liu,¹ Ch. Elster,¹ and W. Glöckle²¹*Institute of Nuclear and Particle Physics and Department of Physics and Astronomy, Ohio University, Athens, Ohio 45701, USA*²*Institute for Theoretical Physics II, Ruhr-University Bochum, D-44780 Bochum, Germany.*

(Received 12 October 2004; revised manuscript received 25 August 2005; published 9 November 2005)

The Faddeev equation for three-body scattering at arbitrary energies is formulated in momentum space and directly solved in terms of momentum vectors without employing a partial-wave decomposition. In its simplest form, the Faddeev equation for identical bosons, which we are using, is a three-dimensional integral equation in five variables, magnitudes of relative momenta and angles. This equation is solved through Padé summation. Based on a Malfliet-Tjon-type potential, the numerical feasibility and stability of the algorithm for solving the Faddeev equation is demonstrated. Special attention is given to the selection of independent variables and the treatment of three-body breakup singularities with a spline-based method. The elastic differential cross section, semiexclusive $d(N, N')$ cross sections, and total cross sections of both elastic and breakup processes in the intermediate-energy range up to about 1 GeV are calculated and the convergence of the multiple-scattering series is investigated in every case. In general, a truncation in the first or second order in the two-body t matrix is quite insufficient.

DOI: [10.1103/PhysRevC.72.054003](https://doi.org/10.1103/PhysRevC.72.054003)

PACS number(s): 21.45.+v

I. INTRODUCTION

During the past two decades calculations of nucleon-deuteron scattering experienced large improvements and refinements. Here, different techniques have been applied: Faddeev calculations in configuration space [1] and momentum space [2], and variational calculations based on a hyperspherical harmonic expansion [3,4]. It is fair to say that below about 200-MeV projectile energy the momentum-space Faddeev equations for three-nucleon scattering can now be solved with high accuracy for the most modern two- and three-nucleon forces. A summary of these achievements can be found in Refs. [5–9]. The approach described there is based on using angular-momentum eigenstates for the two- and three-body systems. This partial-wave decomposition replaces the continuous-angle variables with discrete orbital angular-momentum quantum numbers and thus reduces the number of continuous variables to be discretized in a numerical treatment. For low projectile energies, the procedure of considering orbital angular-momentum components appears physically justified because of arguments related to the centrifugal barrier and the short range of the nuclear force. However, the algebraic and algorithmic steps to be carried out in a partial-wave decomposition can be quite involved when the Faddeev equations on being solved. If one considers three-nucleon scattering at a few hundred mega-electron-volts of projectile energy, the number of partial waves needed to achieve convergence proliferates, and limitations with respect to computational feasibility and accuracy are reached.

It appears therefore natural to avoid a partial-wave representation completely and work directly with vector variables. This is common practice in bound-state calculations of few-nucleon systems based on variational [10] and the Green's function Monte Carlo (GFMC) methods [11–14], which are carried out in configuration space.

Our aim is to work directly with vector variables in the Faddeev scheme in momentum space. In earlier work

[15,16] we showed that the bound-state Faddeev equation has a rather transparent structure when formulated with vector variables compared with the coupled set of two-dimensional integral equations obtained in a partial-wave decomposed form. Based on Malfliet-Tjon-type interactions for two- as well as three-body forces, the numerical solution of the bound state equation using vector variables was demonstrated to be straightforward and numerically very accurate. As far as three-nucleon scattering is concerned, the neutron-deuteron breakup process has been successfully studied up to 500-MeV projectile energy based on the first-order term of the Faddeev equation by use of realistic nucleon-nucleon forces [17].

In this paper we want to show that the full solution of the three-body scattering equation can be obtained in a straightforward manner when vector variables, i.e., magnitudes of momenta and angles between the momentum vectors, are used. As a simplification we neglect spin and isospin degrees of freedom and treat three-boson scattering. The interactions employed are of the Yukawa type, and no separable approximations are involved. The Faddeev equation for three identical bosons is solved exactly as a function of momentum vectors below and above the three-body breakup.

This paper is organized as follows. Section II reviews the Faddeev equation for three-body scattering in momentum space and discusses our choice of momentum and angle variables for the unknown amplitude in the equation and its kernel. In Sec. III we derive the amplitudes and cross sections for elastic-scattering and breakup processes. In addition we relate both by means of the optical theorem. In Sec. IV we discuss the numerical methods necessary for solving the Faddeev equation, especially our treatment of the singularities in the free three-body propagator. In addition, our numerical tests for the solution are shown and discussed. In Sec. V we present calculations for elastic-scattering and breakup processes in the intermediate energy regime from 0.2 to 1 GeV. Our focus here is on the study of the importance of

rescattering terms as function of the projectile energy and the reaction considered. We conclude in Sec. VI.

II. FADDEEV EQUATIONS FOR THREE BOSONS IN THE CONTINUUM

Various presentations of three-body scattering in the Faddeev scheme are presented in the literature [5,6,18]. We solve the Faddeev equation for three identical particles in the form

$$T|\phi\rangle = tP|\phi\rangle + tPG_0T|\phi\rangle. \quad (2.1)$$

The driving term of this integral equation consists of the two-body t matrix t , the sum P of a cyclic and anticyclic permutation of three particles, and the initial state $|\phi\rangle = |\varphi_d \mathbf{q}_0\rangle$, composed of a two-body bound state and the momentum eigenstate of the projectile particle. The kernel of Eq. (2.1) contains the free three-body propagator, $G_0 = (E - H_0 + i\varepsilon)^{-1}$, where E is the total energy in the center-of-mass (c.m.) frame.

The operator T determines both the full breakup amplitude

$$U_0 = (1 + P)T \quad (2.2)$$

and the amplitude for elastic scattering

$$U = PG_0^{-1} + PT. \quad (2.3)$$

In this paper we focus on three identical bosons and use a momentum-space representation. For solving Eq. (2.1), we introduce standard Jacobi momenta \mathbf{p} , the relative momentum in the subsystem, and \mathbf{q} , the relative momentum of the spectator to the subsystem. The momentum states are normalized according to $\langle \mathbf{p}' \mathbf{q}' | \mathbf{p} \mathbf{q} \rangle = \delta^3(\mathbf{p}' - \mathbf{p}) \delta^3(\mathbf{q}' - \mathbf{q})$. Projecting Eq. (2.1) onto Jacobi momenta leads to [19]

$$\begin{aligned} \langle \mathbf{p} \mathbf{q} | T | \varphi_d \mathbf{q}_0 \rangle &= \varphi_d \left(\mathbf{q} + \frac{1}{2} \mathbf{q}_0 \right) t_s \left(\mathbf{p}, \frac{1}{2} \mathbf{q} + \mathbf{q}_0, E - \frac{3}{4m} q^2 \right) \\ &+ \int d^3 q'' t_s \left(\mathbf{p}, \frac{1}{2} \mathbf{q} + \mathbf{q}'', E - \frac{3}{4m} q'^2 \right) \\ &\times \frac{\langle \mathbf{q} + \frac{1}{2} \mathbf{q}'', \mathbf{q}'' | T | \varphi_d \mathbf{q}_0 \rangle}{E - \frac{1}{m}(q^2 + q''^2 + \mathbf{q} \cdot \mathbf{q}'') + i\varepsilon}. \end{aligned} \quad (2.4)$$

Here $t_s(\mathbf{p}', \mathbf{p}) = t(\mathbf{p}, \mathbf{p}') + t(-\mathbf{p}', \mathbf{p})$ is the symmetrized t matrix and E is the total energy in the c.m. system:

$$E = E_d + \frac{3}{4m} q_0^2 = E_d + \frac{2}{3} E_{\text{lab}}. \quad (2.5)$$

We assume that the underlying force is a two-body force, generating t by means of a two-body Lippmann-Schwinger equation and supporting one bound state with energy E_d . Thus $t_s(z)$ has a pole at $z = E_d$. Because the transition operator T in Eq. (2.4) is needed for all values of \mathbf{q} , one encounters this pole of t_s . Extracting the residue explicitly by defining

$$t_s(\mathbf{p}', \mathbf{p}, z) \equiv \frac{\hat{t}_s(\mathbf{p}', \mathbf{p}, z)}{z - E_d} \quad (2.6)$$

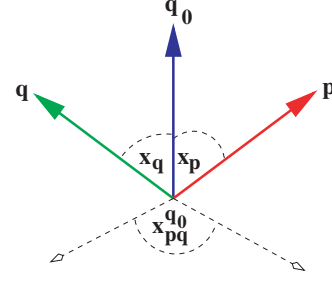


FIG. 1. (Color online) The geometry of three vectors \mathbf{q}_0 , \mathbf{q} , and \mathbf{p} relevant in the three-body scattering problem. The independent-angle variables x_q , x_p , and $x_{pq}^{q_0}$ as defined in Sec. II are indicated. The dashed arrows represent the normal vectors $(\mathbf{q}_0 \times \mathbf{q})$ and $(\mathbf{p} \times \mathbf{q}_0)$.

and similarly for T , one can rewrite Eq. (2.4) as

$$\begin{aligned} \langle \mathbf{p} \mathbf{q} | \hat{T} | \varphi_d \mathbf{q}_0 \rangle &= \varphi_d \left(\mathbf{q} + \frac{1}{2} \mathbf{q}_0 \right) \hat{t}_s \left(\mathbf{p}, \frac{1}{2} \mathbf{q} + \mathbf{q}_0, E - \frac{3}{4m} q^2 \right) \\ &+ \int d^3 q'' \frac{\hat{t}_s \left(\mathbf{p}, \frac{1}{2} \mathbf{q} + \mathbf{q}'', E - \frac{3}{4m} q'^2 \right)}{E - \frac{1}{m}(q^2 + q''^2 + \mathbf{q} \cdot \mathbf{q}'') + i\varepsilon} \\ &\times \frac{\langle \mathbf{q} + \frac{1}{2} \mathbf{q}'', \mathbf{q}'' | \hat{T} | \varphi_d \mathbf{q}_0 \rangle}{E - \frac{3}{4m} q''^2 - E_d + i\varepsilon}. \end{aligned} \quad (2.7)$$

This expression is the starting point for our numerical calculation of the transition amplitude without employing an angular-momentum decomposition.

The first important step for an explicit calculation is the selection of independent variables. Because we ignore spin and isospin dependencies, the matrix element $\langle \mathbf{p} \mathbf{q} | \hat{T} | \varphi_d \mathbf{q}_0 \rangle$ is a scalar function of the variables \mathbf{p} and \mathbf{q} for a given projectile momentum \mathbf{q}_0 . Thus one needs five variables to uniquely specify the geometry of the three vectors \mathbf{p} , \mathbf{q} , and \mathbf{q}_0 , which are shown in Fig. 1. Having in mind that with three vectors one can span two planes, i.e., the $\mathbf{p} - \mathbf{q}_0$ plane and the $\mathbf{q} - \mathbf{q}_0$ plane, a natural choice of independent variables is

$$\begin{aligned} p &= |\mathbf{p}|, \quad q = |\mathbf{q}|, \quad x_p = \hat{\mathbf{p}} \cdot \hat{\mathbf{q}}_0, \quad x_q = \hat{\mathbf{q}} \cdot \hat{\mathbf{q}}_0, \\ x_{pq}^{q_0} &= (\widehat{\mathbf{q}_0 \times \mathbf{q}}) \cdot (\widehat{\mathbf{q}_0 \times \mathbf{p}}). \end{aligned} \quad (2.8)$$

The last variable, $x_{pq}^{q_0}$, is the angle between the two normal vectors of the $\mathbf{p} - \mathbf{q}_0$ plane and the $\mathbf{q} - \mathbf{q}_0$ plane, which are explicitly given by

$$\begin{aligned} (\widehat{\mathbf{q}_0 \times \mathbf{p}}) &= \frac{\hat{\mathbf{q}}_0 \times \hat{\mathbf{p}}}{\sqrt{1 - (\hat{\mathbf{q}}_0 \cdot \hat{\mathbf{p}})^2}}, \\ (\widehat{\mathbf{q}_0 \times \mathbf{q}}) &= \frac{\hat{\mathbf{q}}_0 \times \hat{\mathbf{q}}}{\sqrt{1 - (\hat{\mathbf{q}}_0 \cdot \hat{\mathbf{q}})^2}}. \end{aligned} \quad (2.9)$$

It should be pointed out that the angle between the vectors \mathbf{q} and \mathbf{p} , $y_{pq} = \hat{\mathbf{p}} \cdot \hat{\mathbf{q}}$, is *not* an independent variable. In fact, if x_p and x_q are given, the domain of y_{pq} is bound by

$$x_p x_q - \sqrt{1 - x_p^2} \sqrt{1 - x_q^2} \leq y_{pq} \leq x_p x_q + \sqrt{1 - x_p^2} \sqrt{1 - x_q^2}, \quad (2.10)$$

thus not covering the entire interval $[-1, 1]$. Using the explicit representation of the normal vectors and standard

cross-product identities, we arrive at the following relation between $x_{pq}^{q_0}$ and y_{pq} :

$$\begin{aligned} x_{pq}^{q_0} &= \frac{\hat{\mathbf{p}} \cdot \hat{\mathbf{q}} - (\hat{\mathbf{q}}_0 \cdot \hat{\mathbf{p}})(\hat{\mathbf{q}}_0 \cdot \hat{\mathbf{q}})}{\sqrt{1 - (\hat{\mathbf{q}}_0 \cdot \hat{\mathbf{p}})^2} \sqrt{1 - (\hat{\mathbf{q}}_0 \cdot \hat{\mathbf{q}})^2}} \\ &= \frac{y_{pq} - x_p x_q}{\sqrt{1 - x_p^2} \sqrt{1 - x_q^2}}, \end{aligned} \quad (2.11)$$

or

$$y_{pq} = x_p x_q + \sqrt{1 - x_p^2} \sqrt{1 - x_q^2} x_{pq}^{q_0}. \quad (2.12)$$

For the special case in which $\hat{\mathbf{q}}_0$ is parallel to the z axis (q_0 system), one can write

$$y_{pq} = x_p x_q + \sqrt{1 - x_p^2} \sqrt{1 - x_q^2} \cos \varphi_{pq}, \quad (2.13)$$

where φ_{pq} is the difference of the azimuthal angles of $\hat{\mathbf{p}}$ and $\hat{\mathbf{q}}$. However, the variable $\cos \varphi_{pq}$, which was used erroneously in [19] as the third angular variable, is not rotationally invariant.

With the independent variables listed in Eqs. (2.8), the matrix element of \hat{T} is given as

$$\langle \mathbf{p}\mathbf{q} | \hat{T} | \hat{\mathbf{p}}\mathbf{q}_0 \rangle \equiv \hat{T}(p, x_p, x_{pq}^{q_0}, x_q, q; q_0). \quad (2.14)$$

Furthermore, $\hat{t}_s(\mathbf{p}', \mathbf{p}, z)$ is also a scalar function and thus can be written in the form

$$\hat{t}_s(\mathbf{p}', \mathbf{p}, z) = \hat{t}_s(p', p, \hat{\mathbf{p}}' \cdot \hat{\mathbf{p}}, z). \quad (2.15)$$

The most intricate dependence appears under the integral in Eq. (2.7) for the third angular variable of the \hat{T} amplitude. According to Eq. (2.11) it is given as

$$x_{(q+\frac{1}{2}q'')q''}^{q_0} \equiv \frac{\left(\mathbf{q} + \frac{1}{2}\mathbf{q}''\right) \cdot \hat{\mathbf{q}}'' - \hat{\mathbf{q}}_0 \cdot \left(\mathbf{q} + \frac{1}{2}\mathbf{q}''\right) \hat{\mathbf{q}}_0 \cdot \hat{\mathbf{q}}''}{\sqrt{1 - \left[\hat{\mathbf{q}}_0 \cdot \left(\mathbf{q} + \frac{1}{2}\mathbf{q}''\right)\right]^2} \sqrt{1 - (\hat{\mathbf{q}}_0 \cdot \hat{\mathbf{q}}'')^2}}. \quad (2.16)$$

In view of the breakup singularities of the first denominator in Eq. (2.7) it is mandatory to choose the coordinate system for the \mathbf{q}'' integration such that the z axis points parallel to the vector $\hat{\mathbf{q}}$. Then one obtains for Eq. (2.16)

$$x_{(q+\frac{1}{2}q'')q''}^{q_0} = \frac{\frac{qx'' + \frac{1}{2}q''}{\sqrt{q^2 + \frac{1}{4}q''^2 + qq''x''}} - x_{q+\frac{1}{2}q''} x_{q''}}{\sqrt{1 - x_{q+\frac{1}{2}q''}^2} \sqrt{1 - x_{q''}^2}}, \quad (2.17)$$

where

$$x_{q''} \equiv \hat{\mathbf{q}}'' \cdot \hat{\mathbf{q}}_0 = x'' x_q + \sqrt{1 - x''^2} \sqrt{1 - x_q^2} \cos(\varphi'' - \varphi_{q_0}),$$

$$x_{q+\frac{1}{2}q''} \equiv \left(\mathbf{q} + \frac{1}{2}\mathbf{q}''\right) \cdot \hat{\mathbf{q}}_0 = \frac{qx_q + \frac{1}{2}q''x_{q''}}{\sqrt{q^2 + \frac{1}{4}q''^2 + qq''x''}}. \quad (2.18)$$

Here φ_{q_0} is the azimuthal angle of $\hat{\mathbf{q}}_0$ in the coordinate system chosen for the \mathbf{q}'' integration. These considerations lead to the explicit representation for the transition amplitude \hat{T} :

$$\begin{aligned} \hat{T}(p, x_p, x_{pq}^{q_0}, x_q, q; q_0) &= \varphi_d \left(\sqrt{q^2 + \frac{1}{4}q_0^2 + qq_0x_q} \right) \\ &\times \hat{t}_s \left(p, \sqrt{\frac{1}{4}q^2 + q_0^2 + qq_0x_q}, \frac{\frac{1}{2}qy_{pq} + q_0x_p}{\sqrt{\frac{1}{4}q^2 + q_0^2 + qq_0x_q}}; E - \frac{3}{4m}q^2 \right) \\ &+ \int_0^\infty dq'' q''^2 \int_{-1}^{+1} dx'' \int_0^{2\pi} d\varphi'' \frac{1}{E - \frac{1}{m}(q^2 + qq''x'' + q''^2) + i\varepsilon} \\ &\times \hat{t}_s \left(p, \sqrt{\frac{1}{4}q^2 + q''^2 + qq''x''}, \frac{\frac{1}{2}qy_{pq} + q''y_{pq''}}{\sqrt{\frac{1}{4}q^2 + q''^2 + qq''x''}}; E - \frac{3}{4m}q^2 \right) \\ &\times \frac{\hat{T} \left(\sqrt{q^2 + \frac{1}{4}q''^2 + qq''x''}, \frac{qx_q + \frac{1}{2}q''x_{q''}}{\sqrt{q^2 + \frac{1}{4}q''^2 + qq''x''}}, \frac{\frac{qx'' + \frac{1}{2}q''}{\sqrt{q^2 + \frac{1}{4}q''^2 + qq''x''}} - x_{q+\frac{1}{2}q''} x_{q''}}{\sqrt{1 - x_{q+\frac{1}{2}q''}^2} \sqrt{1 - x_{q''}^2}}, x_{q''}, q''; q_0 \right)}{E - \frac{3}{4m}q''^2 - E_d + i\varepsilon}, \end{aligned} \quad (2.19)$$

where, in addition to Eqs. (2.8) and the related variables of Eqs. (2.12) and (2.18), the following variables occur:

$$\begin{aligned} q'' &= |\mathbf{q}''|, \\ x'' &= \hat{\mathbf{q}} \cdot \hat{\mathbf{q}}'', \\ y_{pq''} &= \hat{\mathbf{p}} \cdot \hat{\mathbf{q}}'' = y_{pq} x'' + \sqrt{1 - x''^2} \sqrt{1 - y_{pq}^2} \cos(\varphi_p - \varphi''). \end{aligned} \quad (2.20)$$

Like φ_{q_0} in Eqs. (2.18), the angle φ_p in Eqs. (2.20) is the azimuthal angle of $\hat{\mathbf{p}}$ in the q system (i.e., the system in which the z axis is parallel to $\hat{\mathbf{q}}$). It remains to relate the angles φ_p and φ_{q_0} to the three angular variables $x_p, x_q,$ and $x_{pq}^{q_0}$. As shown in the Appendix, because of the φ'' integration, only the knowledge of $\cos(\varphi_p - \varphi_{q_0})$ is required. As $\cos \varphi_{pq}$ in Eq. (2.13) is equal to $x_{pq}^{q_0}$ in the q_0 system, so too is

$\cos(\varphi_p - \varphi_{q_0})$ equal to $x_{q_0 p}^q$ in the q system. Thus

$$\begin{aligned} \cos(\varphi_p - \varphi_{q_0}) &= x_{q_0 p}^q = \frac{\hat{\mathbf{q}}_0 \cdot \hat{\mathbf{p}} - (\hat{\mathbf{q}} \cdot \hat{\mathbf{q}}_0)(\hat{\mathbf{q}} \cdot \hat{\mathbf{p}})}{\sqrt{1 - (\hat{\mathbf{q}} \cdot \hat{\mathbf{q}}_0)^2} \sqrt{1 - (\hat{\mathbf{p}} \cdot \hat{\mathbf{q}})^2}} \\ &= \frac{x_p - x_q y_{pq}}{\sqrt{1 - x_q^2} \sqrt{1 - y_{pq}^2}}. \end{aligned} \quad (2.21)$$

Because of that difference ($\varphi_p - \varphi_{q_0}$), one can choose φ_{q_0} arbitrarily, e.g., zero. Furthermore, $\cos \varphi_p$ and $\sin \varphi_p$ required in Eqs. (2.20) are given in terms of $\cos(\varphi_p - \varphi_{q_0})$, as is shown in the Appendix. This completes the definition of all relevant variables in Eq. (2.19).

III. AMPLITUDES AND CROSS SECTIONS FOR ELASTIC-SCATTERING AND BREAKUP PROCESSES

The amplitude for elastic scattering is obtained by calculation of the matrix element of the operator U given in Eq. (2.3) as

$$\begin{aligned} \langle \mathbf{q} \varphi_d | U | \mathbf{q}_0 \varphi_d \rangle &= 2\varphi_d \left(\frac{1}{2} \mathbf{q} + \mathbf{q}_0 \right) \left[E - \frac{1}{m} (q^2 + \mathbf{q} \cdot \mathbf{q}_0 + q_0^2) \right] \\ &\times \varphi_d \left(\mathbf{q} + \frac{1}{2} \mathbf{q}_0 \right) + 2 \int d^3 q'' \varphi_d \left(\frac{1}{2} \mathbf{q} + \mathbf{q}'' \right) \\ &\times \frac{\langle \mathbf{q} + \frac{1}{2} \mathbf{q}'', \mathbf{q}'' | \hat{T} | \mathbf{q}_0 \varphi_d \rangle}{E - \frac{3}{4m} q''^2 - E_d + i\varepsilon}. \end{aligned} \quad (3.1)$$

The amplitude for the full breakup process according to Eq. (2.2) is given by

$$\begin{aligned} \langle \mathbf{p} \mathbf{q} | U_0 | \mathbf{q}_0 \varphi_d \rangle &= \frac{\langle \mathbf{p} \mathbf{q} | \hat{T} | \mathbf{q}_0 \varphi_d \rangle}{E - \frac{3}{4m} \mathbf{q}^2 - E_d} \\ &+ \frac{\langle -\frac{1}{2} \mathbf{p} + \frac{3}{4} \mathbf{q}, -\mathbf{p} - \frac{1}{2} \mathbf{q} | \hat{T} | \mathbf{q}_0 \varphi_d \rangle}{E - \frac{3}{4m} (-\mathbf{p} - \frac{1}{2} \mathbf{q})^2 - E_d} \\ &+ \frac{\langle -\frac{1}{2} \mathbf{p} - \frac{3}{4} \mathbf{q}, \mathbf{p} - \frac{1}{2} \mathbf{q} | \hat{T} | \mathbf{q}_0 \varphi_d \rangle}{E - \frac{3}{4m} (\mathbf{p} - \frac{1}{2} \mathbf{q})^2 - E_d}. \end{aligned} \quad (3.2)$$

The equation for the elastic operator U follows from Eqs. (2.1) and (2.3). It is given as

$$U|\phi\rangle = P G_0^{-1} |\phi\rangle + P t G_0 U |\phi\rangle. \quad (3.3)$$

Straightforward and well-known steps [5] based on this equation lead to the unitarity relation

$$\begin{aligned} \langle \phi | U | \phi' \rangle^* - \langle \phi' | U | \phi \rangle &= \int d^3 q \langle \phi_q | U | \phi' \rangle^* 2\pi i \\ &\times \delta \left(E - E_d - \frac{3}{4m} q^2 \right) \langle \phi_q | U | \phi \rangle \\ &+ \frac{1}{3} \int d^3 p d^3 q \langle \phi_0 | U_0 | \phi' \rangle^* 2\pi i \\ &\times \delta \left(E - \frac{p^2}{m} - \frac{3}{4m} q^2 \right) \langle \phi_0 | U_0 | \phi \rangle. \end{aligned} \quad (3.4)$$

We point out that there is a misprint in Eq. (202) of Ref. [5]: The factor 1/3 is missing.

Using the variables defined in the previous section and having in mind that for elastic scattering $|\mathbf{q}| = |\mathbf{q}_0|$, one can express the amplitude for elastic scattering according to Eq. (3.1) as

$$\begin{aligned} \langle \mathbf{q} \varphi_d | U | \mathbf{q}_0 \varphi_d \rangle &\equiv U(q_0, x_q) \\ &= 2\varphi_d^2 \left(q_0 \sqrt{\frac{5}{4} + x_q} \right) \left[E - \frac{q_0^2}{m} (2 + x_q) \right] \\ &+ 2 \int_0^\infty dq'' q''^2 \int_{-1}^{+1} dx'' \int_0^{2\pi} d\varphi'' \\ &\times \frac{1}{E - \frac{3}{4m} q''^2 - E_d + i\varepsilon} \\ &\times \varphi_d \left(\sqrt{\frac{1}{4} q_0^2 + q''^2 + q_0 q'' y_{q q''}} \right) \\ &\times \hat{T} \left(\sqrt{q_0^2 + \frac{1}{4} q''^2 + q_0 q'' y_{q q''}}, \right. \\ &\quad \left. \frac{q_0 x_q + \frac{1}{2} q'' y_{q_0 q''}}{\sqrt{q_0^2 + \frac{1}{4} q''^2 + q_0 q'' y_{q q''}}}, \right. \\ &\quad \left. \frac{q_0 y_{q q''} + \frac{1}{2} q''}{\sqrt{q_0^2 + \frac{1}{4} q''^2 + q_0 q'' y_{q q''}}} - x_{\pi_p} x_{\pi_q}, \right. \\ &\quad \left. \frac{y_{q_0 q''}, q''; q_0}{\sqrt{1 - x_{\pi_p}^2} \sqrt{1 - x_{\pi_q}^2}} \right). \end{aligned} \quad (3.5)$$

with

$$\begin{aligned} y_{q q''} &= \hat{\mathbf{q}} \cdot \hat{\mathbf{q}}'', \\ y_{q_0 q''} &= \hat{\mathbf{q}}_0 \cdot \hat{\mathbf{q}}'' = x_{\pi_q}, \\ x_{\pi_p} &= \frac{q_0 x_q + \frac{1}{2} q'' y_{q_0 q''}}{\sqrt{q_0^2 + \frac{1}{4} q''^2 + q_0 q'' y_{q q''}}}. \end{aligned} \quad (3.6)$$

At this point, the choice of a specific coordinate system for the \mathbf{q}'' integration is still open. The angular variable $x_q = \hat{\mathbf{q}} \cdot \hat{\mathbf{q}}_0$ represents the scattering angle. If the z axis is chosen parallel to $\hat{\mathbf{q}}_0$, the angles are

$$\begin{aligned} y_{q q''} &= x_q x'' + \sqrt{1 - x_q^2} \sqrt{1 - x''^2} \cos(\varphi_q - \varphi''), \\ y_{q_0 q''} &= x''. \end{aligned} \quad (3.7)$$

While having the z axis parallel to $\hat{\mathbf{q}}_0$ may be the intuitive choice to describe the scattering with a given beam direction, we can in principle also choose the z axis parallel to $\hat{\mathbf{q}}$. In that case the angles in Eqs. (3.6) are given by

$$\begin{aligned} y_{q q''} &= x'', \\ y_{q_0 q''} &= x_q x'' + \sqrt{1 - x_q^2} \sqrt{1 - x''^2} \cos(\varphi_{q_0} - \varphi''). \end{aligned} \quad (3.8)$$

The elastic cross section depends on the angle between the vectors $\hat{\mathbf{q}}_0$ and $\hat{\mathbf{q}}$, but not on the choice of the z axis. We use the possibility of calculating the matrix elements of U in the two different coordinate systems to test the quality of our numerical calculations.

The differential elastic cross section in the c.m. frame is given by

$$\frac{d\sigma_{\text{el}}}{d\Omega} = \left(\frac{2m}{3}\right)^2 (2\pi)^4 |U(q_0 x_q)|^2, \quad (3.9)$$

and the corresponding total elastic cross section is

$$\sigma_{\text{el}} = \int d\Omega \frac{d\sigma_{\text{el}}}{d\Omega} = \left(\frac{2m}{3}\right)^2 (2\pi)^5 \int_{-1}^{+1} dx |U(q_0, x)|^2. \quad (3.10)$$

The full breakup amplitude is given in Eq. (3.2). On the energy shell, p and q are constrained by $p^2 + \frac{3}{4}q^2 = mE$. As a function of all five variables and the projectile momentum it reads

$$\begin{aligned} U_0(p, x_p, x_{pq}^{q_0}, x_q, q, q_0) = & \frac{\hat{T}(p, x_p, x_{pq}^{q_0}, x_q, q, q_0)}{E - \frac{3}{4m}q^2 - E_d} \\ & + \frac{\hat{T}(p_2, x_{p_2}, x_{p_2 q_2}^{q_0}, x_{q_2}, q_2, q_0)}{E - \frac{3}{4m}q_2^2 - E_d} \\ & + \frac{\hat{T}(p_3, x_{p_3}, x_{p_3 q_3}^{q_0}, x_{q_3}, q_3, q_0)}{E - \frac{3}{4m}q_3^2 - E_d}. \end{aligned} \quad (3.11)$$

Here the variables are defined as

$$\begin{aligned} x_{pq} &= x_p x_q + \sqrt{1 - x_p^2} \sqrt{1 - x_q^2} x_{pq}^{q_0}, \\ p_2 &= \left| -\frac{1}{2}\mathbf{p} + \frac{3}{4}\mathbf{q} \right| = \frac{1}{2} \sqrt{p^2 + \frac{9}{4}q^2 - 3pqy_{pq}}, \\ q_2 &= \left| -\mathbf{p} - \frac{1}{2}\mathbf{q} \right| = \sqrt{p^2 + \frac{1}{4}q^2 + pqy_{pq}}, \\ p_3 &= \left| -\frac{1}{2}\mathbf{p} - \frac{3}{4}\mathbf{q} \right| = \frac{1}{2} \sqrt{p^2 + \frac{9}{4}q^2 + 3pqy_{pq}}, \\ q_3 &= \left| +\mathbf{p} - \frac{1}{2}\mathbf{q} \right| = \sqrt{p^2 + \frac{1}{4}q^2 - pqy_{pq}}, \\ x_{p_2} &= \hat{\mathbf{p}}_2 \cdot \hat{\mathbf{q}}_0 = \frac{-\frac{1}{2}px_p + \frac{3}{4}qx_q}{p_2}, \\ x_{q_2} &= \hat{\mathbf{q}}_2 \cdot \hat{\mathbf{q}}_0 = \frac{-px_p - \frac{1}{2}qx_q}{q_2}, \\ x_{p_3} &= \hat{\mathbf{p}}_3 \cdot \hat{\mathbf{q}}_0 = \frac{-\frac{1}{2}px_p - \frac{3}{4}qx_q}{p_3}, \\ x_{q_3} &= \hat{\mathbf{q}}_3 \cdot \hat{\mathbf{q}}_0 = \frac{+px_p - \frac{1}{2}qx_q}{q_3}, \\ x_{p_2 q_2}^{q_0} &= (\hat{\mathbf{q}}_0 \times \hat{\mathbf{p}}_2) \cdot (\hat{\mathbf{q}}_0 \times \hat{\mathbf{q}}_2) = \frac{\frac{1}{2}p^2 - \frac{3}{8}q^2 - \frac{1}{2}pqy_{pq} - x_{p_2}x_{q_2}}{p_2 q_2}, \\ x_{p_3 q_3}^{q_0} &= (\hat{\mathbf{q}}_0 \times \hat{\mathbf{p}}_3) \cdot (\hat{\mathbf{q}}_0 \times \hat{\mathbf{q}}_3) = \frac{-\frac{1}{2}p^2 + \frac{3}{8}q^2 - \frac{1}{2}pqy_{pq} - x_{p_3}x_{q_3}}{p_3 q_3}. \end{aligned} \quad (3.12)$$

The fivefold differential breakup cross section is given in the c.m. frame:

$$\begin{aligned} \frac{d^5\sigma_{\text{br}}}{d\Omega_p d\Omega_q dq} = & \frac{(2\pi)^4 m^2}{3q_0} q^2 \sqrt{mE - \frac{3}{4}q^2} \\ & \times |U_0(p, x_p, x_{pq}^{q_0}, x_q, q, q_0)|^2. \end{aligned} \quad (3.13)$$

It is convenient to calculate the total breakup cross section in the c.m. frame as there are no kinematic restrictions on the relative angles. For the explicit calculation we can make different choices of the z axis, e.g., it can be parallel to the direction $\hat{\mathbf{q}}_0$ of the projectile or parallel to either one of the Jacobi vectors $\hat{\mathbf{q}}$ and $\hat{\mathbf{p}}$. The different choices will obviously result in different angular integrations. For completeness we give all three choices here. This will be used as a highly nontrivial test of the numerical results, as will be demonstrated in the next section. If the z axis is parallel to $\hat{\mathbf{q}}_0$ we have

$$\int d\Omega_p d\Omega_q = 2\pi \int_{-1}^{+1} dx_p'' \int_{-1}^{+1} dx_q'' \int_0^{2\pi} d\varphi_{pq}'', \quad (3.14)$$

with

$$x_p \rightarrow x_p'', \quad x_q \rightarrow x_q'', \quad x_{pq}^{q_0} \rightarrow \cos \varphi_{pq}''. \quad (3.15)$$

If the z axis is parallel to $\hat{\mathbf{q}}$, the angular integration becomes

$$\int d\Omega_p d\Omega_q = 2\pi \int_{-1}^{+1} dx_q'' \int_{-1}^{+1} dy_{pq}'' \int_0^{2\pi} d\varphi_{pq_0}'', \quad (3.16)$$

with

$$\begin{aligned} x_p &\rightarrow x_q'' y_{pq}'' + \sqrt{1 - x_q''^2} \sqrt{1 - y_{pq}''^2} \cos \varphi_{pq_0}'', \\ x_q &\rightarrow x_q'', \end{aligned} \quad (3.17)$$

$$x_{pq}^{q_0} \rightarrow \frac{y_{pq}'' - \left(x_q'' y_{pq}'' + \sqrt{1 - x_q''^2} \sqrt{1 - y_{pq}''^2} \cos \varphi_{pq_0}'' \right) x_q''}{\sqrt{1 - \left(x_q'' y_{pq}'' + \sqrt{1 - x_q''^2} \sqrt{1 - y_{pq}''^2} \cos \varphi_{pq_0}'' \right)^2} \sqrt{1 - x_q''^2}}.$$

Finally, if the z axis is parallel to $\hat{\mathbf{p}}$, the angular integration is

$$\int d\Omega_p d\Omega_q = 2\pi \int_{-1}^{+1} dx_p'' \int_{-1}^{+1} dy_{pq}'' \int_0^{2\pi} d\varphi_{q_0}'', \quad (3.18)$$

with

$$\begin{aligned} x_p &\rightarrow x_p'', \\ x_q &\rightarrow x_p'' y_{pq}'' + \sqrt{1 - x_p''^2} \sqrt{1 - y_{pq}''^2} \cos \varphi_{q_0}'', \end{aligned} \quad (3.19)$$

$$x_{pq}^{q_0} \rightarrow \frac{y_{pq}'' - \left(x_p'' y_{pq}'' + \sqrt{1 - x_p''^2} \sqrt{1 - y_{pq}''^2} \cos \varphi_{q_0}'' \right) x_p''}{\sqrt{1 - \left(x_p'' y_{pq}'' + \sqrt{1 - x_p''^2} \sqrt{1 - y_{pq}''^2} \cos \varphi_{q_0}'' \right)^2} \sqrt{1 - x_p''^2}}.$$

Let us define a function $\mathcal{F}(p, q)$ as

$$\mathcal{F}(p, q) = \int d\Omega_p d\Omega_q |\langle \phi_0 | U_0 | \phi \rangle|^2, \quad (3.20)$$

where the angle integrations over the breakup amplitude are carried out. This function should be independent of the coordinate system in which the angle integrations are performed. We use this property to check our numerical calculations. This is a nontrivial test of our calculation because,

especially at higher energies, the transition amplitude \hat{T} develops stronger angle dependencies, which challenge the accuracy of the multidimensional interpolations.

The angle-integrated breakup cross section is given as

$$\frac{d\sigma_{\text{br}}}{dq} = \frac{1}{3} \frac{(2\pi)^4 m^2}{3q_0} q^2 \sqrt{mE - \frac{3}{4}q^2} \mathcal{F}\left(\sqrt{mE - \frac{3}{4}q^2}, q\right), \quad (3.21)$$

and the total breakup cross section reads

$$\sigma_{\text{br}} = \frac{1}{3} \frac{(2\pi)^4 m^2}{3q_0} \int_0^{\sqrt{\frac{4mE}{3}}} dq q^2 \sqrt{mE - \frac{3}{4}q^2} \times \mathcal{F}\left(\sqrt{mE - \frac{3}{4}q^2}, q\right). \quad (3.22)$$

Using now the unitarity relation from Eq. (3.4), the optical theorem gives

$$\sigma_{\text{tot}} = \sigma_{\text{el}} + \sigma_{\text{br}} = -\frac{4m(2\pi)^3}{3q_0} \text{Im} U(q_0, 1). \quad (3.23)$$

For later use we also mention the semiexclusive cross section, in which only one particle is detected in the breakup process:

$$\frac{d\sigma}{d\Omega_q dq} = (2\pi)^4 \frac{m^2}{3q_0} p q^2 \int d\hat{p} |U_0(p, x_p, x_{pq}^{q_0}, x_q, q, q_0)|^2. \quad (3.24)$$

IV. NUMERICAL METHODS

The fully off-shell two-body t matrix $t(\mathbf{p}', \mathbf{p}, z)$ is solved directly from the Lippmann-Schwinger equation as a function of its vector variables [20] for the off-shell energies $E - (3/4m)q^2$ as required by Eq. (2.4). The Faddeev equation is iterated, generating the multiple-scattering series, which is then summed by the Padé method [21,22]. We use it in the form of a continued fraction expansion as laid out in Ref. [18].

The first integration to be performed in solving Eq. (2.19) by iteration is the integration over the azimuthal angle φ'' . This leads to a function of variables q'' and x'' and requires interpolation in the second and third arguments of t_s and the first four arguments of \hat{T} . Our spline interpolations are based on the cubic Hermite splines given in Ref. [23].

Let $F(q'', x'')$ be the resulting function in each step of the iteration. Clearly it depends in addition on the fixed variables p, q, x_p, x_q , and $x_{pq}^{q_0}$, which are omitted for clarity. Then the next task is performing the remaining two singular integrations:

$$I = \int_0^\infty dq'' q''^2 \int_{-1}^{+1} dx'' \times \frac{F(q'', x'')}{\left[E - \frac{1}{m}(q^2 + q''^2 + qq''x'') + i\varepsilon\right] \left[E - \frac{3}{4m}q''^2 - E_d + i\varepsilon\right]}. \quad (4.1)$$

If the c.m. energy E is below the three-body breakup threshold, only the second denominator is singular, and the simple pole can be treated by standard subtraction methods.

The intricate problem arises above the three-body breakup threshold, when, in addition, the first denominator can vanish. It has the form

$$\frac{1}{E - \frac{1}{m}(q^2 + qq''x'' + q''^2) + i\varepsilon} = \frac{\frac{m}{qq''}}{x_0 - x'' + i\varepsilon}, \quad (4.2)$$

with

$$x_0 = \frac{mE - q^2 - q''^2}{qq''}. \quad (4.3)$$

For $|x_0| \leq 1$, a so-called moving singularity arises in the q'' - x'' integration, as x_0 depends on q . The direct treatment of those moving singularities by use of real variables has been discussed in the literature [2]. We briefly review the appearance of these singularities in form of logarithms, as we introduce a new quasi-analytic integration based on spline functions. The condition $|x_0| = 1$ leads to the pole positions,

$$q'' = \pm \frac{q}{2} \pm \sqrt{mE - \frac{3}{4}q^2}, \quad (4.4)$$

and one arrives at the well-known shape in the q - q'' plane for $|x_0| \leq 1$, shown in Fig. 2. This region is bounded by

$$q_+ = \frac{q}{2} + \sqrt{Q_0^2 - \frac{3}{4}q^2} \quad (4.5)$$

and

$$q_- = \begin{cases} -\frac{q}{2} + \sqrt{Q_0^2 - \frac{3}{4}q^2}, & q < Q_0 \\ +\frac{q}{2} - \sqrt{Q_0^2 - \frac{3}{4}q^2}, & q > Q_0 \end{cases}, \quad (4.6)$$

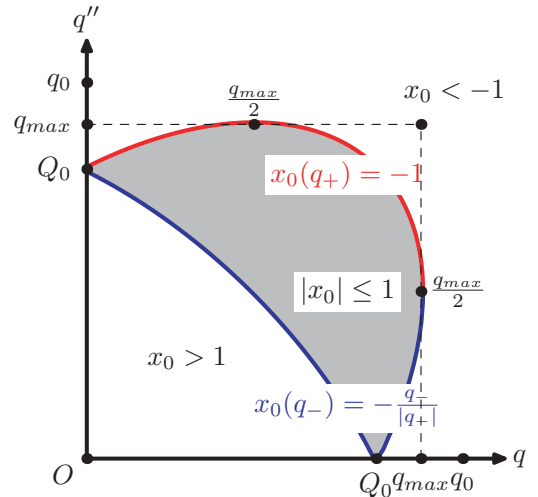


FIG. 2. (Color online) The region of singularities of the free three-particle propagator as a function of the momenta q and q'' . The shaded area in the q - q'' plane indicates the region where $|x_0| \leq 1$, i.e., the region where a pole in the x'' integration occurs. This region is enclosed by the bounding curves q_+ and q_- , which contain the logarithmic singularity as a function of q'' as given in Eqs. (4.5) and (4.6).

where $Q_0 = \sqrt{mE}$. Apparently there is no singularity if $q > q_{\max} \equiv \sqrt{(4m/3)E}$. We distinguish four cases, $q = 0$, $0 < q < q_{\max}$, $q = q_{\max}$, and $q > q_{\max}$. The case $q = 0$ reduces to a simple subtraction and is not discussed. For $0 < q < q_{\max}$ we consider only the part of the q'' integration that contains the moving singularities. It has the schematic form

$$I' = \int_0^{q_{\max}} dq'' \int_{-1}^{+1} dx'' \frac{f(q'', x'')}{x_0 - x'' + i\varepsilon}. \quad (4.7)$$

The first step is to perform a subtraction of the pole, which we carry out in the entire square $0 \leq q, q'' \leq q_{\max}$ by defining

$$\hat{f}(q'', x_0) = \begin{cases} f(q'', x_0) : |x_0| \leq 1 \\ f(q'', \frac{x_0}{|x_0|}) : |x_0| > 1 \end{cases}. \quad (4.8)$$

We obtain

$$\begin{aligned} I' &= \int_0^{q_{\max}} dq'' \int_{-1}^{+1} dx'' \frac{f(q'', x'') - \hat{f}(q'', x_0)}{x_0 - x''} \\ &+ \int_0^{q_{\max}} dq'' \hat{f}(q'', x_0) \ln \left| \frac{1+x_0}{1-x_0} \right| \\ &- i\pi \int_0^{q_{\max}} dq'' \Theta(1 - |x_0|) \hat{f}(q'', x_0), \end{aligned} \quad (4.9)$$

Where Θ is the Heaviside unit step function. Now we define $q_- = \frac{q}{2} - \sqrt{Q_0^2 - \frac{3}{4}q^2}$ and obtain

$$\begin{aligned} \ln \left| \frac{1+x_0}{1-x_0} \right| &= \left(-\frac{q_-}{|q_-|} \ln |q'' + |q_-|| - \ln |q'' + q_+| \right) \\ &+ \left(+\frac{q_-}{|q_-|} \ln |q'' - |q_-|| + \ln |q'' - q_+| \right). \end{aligned} \quad (4.10)$$

This leads to the well-separated part of the integral that contains the logarithmic singularity

$$\int_0^{q_{\max}} dq'' \hat{f}(q'', x_0) \left(+\frac{q_-}{|q_-|} \ln |q'' - |q_-|| + \ln |q'' - q_+| \right). \quad (4.11)$$

It is here that we introduce the new technique that relies on cubic-spline integration.

We divide the range of integration $[0, q_{\max}]$ into intervals bounded by a set of grid points q_i . The set of grid points is supposed to be dense enough to interpolate the function $\hat{f}(q'', x_0) \equiv f(q'')$ sufficiently well by cubic Hermite splines [23]. In Ref. [23] a detailed presentation of these spline functions is given specifically for our use. For the convenience of the reader we now switch to the notation of Ref. [23] and denote the end points of the i th interval by x_1 and x_2 and the two adjacent grid points to the left and right of the i th interval by x_0 and x_3 , respectively. Then, as detailed in Ref. [23], the interpolating function in the i th interval [replacing $f(q'') \equiv f(x)$] can be written as

$$f_i(x) = \sum_{j=0}^3 S_j(x) f(x_j), \quad (4.12)$$

where the modified spline functions are

$$\begin{aligned} S_0(x) &= -\phi_3(x) \frac{x_2 - x_1}{x_1 - x_0} \frac{1}{x_2 - x_0}, \\ S_1(x) &= \phi_1(x) + \phi_3 \left(\frac{x_2 - x_1}{x_1 - x_0} - \frac{x_1 - x_0}{x_2 - x_1} \right) \frac{1}{x_2 - x_0} \\ &- \phi_4(x) \frac{x_3 - x_2}{x_2 - x_1} \frac{1}{x_3 - x_1}, \\ S_2(x) &= \phi_2(x) + \phi_3 \frac{x_1 - x_0}{x_2 - x_1} \frac{1}{x_2 - x_0} \\ &+ \phi_4(x) \left(\frac{x_3 - x_2}{x_2 - x_1} - \frac{x_2 - x_1}{x_3 - x_2} \right) \frac{1}{x_3 - x_1}, \\ S_3(x) &= \phi_4(x) \frac{x_2 - x_1}{x_3 - x_2} \frac{1}{x_3 - x_1}, \end{aligned} \quad (4.13)$$

with

$$\begin{aligned} \phi_1(x) &= \frac{(x_2 - x)^2}{(x_2 - x_1)^3} [(x_2 - x_1) + 2(x - x_1)], \\ \phi_2(x) &= \frac{(x_1 - x)^2}{(x_2 - x_1)^3} [(x_2 - x_1) + 2(x_2 - x)], \\ \phi_3(x) &= \frac{(x - x_1)(x_2 - x)^2}{(x_2 - x_1)^2}, \\ \phi_4(x) &= \frac{(x - x_1)^2(x - x_2)}{(x_2 - x_1)^2}. \end{aligned} \quad (4.14)$$

Therefore, in view of Eqs. (4.11)–(4.14), the following integrals occur for $i = 1 \dots 4$:

$$\begin{aligned} \bar{\phi}_1 &= \int_{x_i}^{x_{i+1}} \phi_1 \ln |x - q| dx, \\ \bar{\phi}_2 &= \int_{x_i}^{x_{i+1}} \phi_2 \ln |x - q| dx, \\ \bar{\phi}_3 &= \int_{x_i}^{x_{i+1}} \phi_3 \ln |x - q| dx, \\ \bar{\phi}_4 &= \int_{x_i}^{x_{i+1}} \phi_4 \ln |x - q| dx, \end{aligned} \quad (4.15)$$

with $q = |q_-|, q_+$. Consequently the five different cases, $q < x_i < x_{i+1}$, $q = x_i < x_{i+1}$, $x_i < q < x_{i+1}$, $x_i < q = x_{i+1}$, and $x_i < x_{i+1} < q$, occur. Because the functions $\phi_i(x)$ are cubic polynomials, the integrals in Eqs. (4.15) can be performed analytically. We leave the explicit calculation to the interested practitioner and refer to Ref. [24] for a detailed presentation. According to our experience, that manner of integrating the moving logarithmic singularities is a very good alternative to the more common subtraction method [2].

Finally, for $q = q_{\max}$, we also apply the subtraction over the extended region $0 \leq q'' \leq q_{\max}$. In that case $q_+ = q_- = (q_{\max}/2)$ and when $q'' = (q_{\max}/2)$ then $x_0 = -1$. Analogous steps lead to that part of the integral, which contains the logarithmic singularity

$$\int_0^{q_{\max}} dq'' \hat{f}(q'', -1) \ln \left| q'' - \frac{q_{\max}}{2} \right|, \quad (4.16)$$

and which is again evaluated by spline-based integration.

To test the correctness as well as the accuracy of our calculations we carried out a variety of numerical tests. Unfortunately we could not compare our work with that of other groups because, to the best of our knowledge, no comparable work at higher energies exists.

Apart from the projectile momentum q_0 , the amplitude \hat{T} of Eq. (2.19) depends on five variables $p, x_p, x_{pq}^{q_0}, x_q$, and q . In addition, there are the integration variables q'', x'' , and φ'' . All calculations listed are based on the Malfliet-Tjon-type potential, which is explicitly given in the next section. The fully off-shell two-body t matrix, $t(p', p, x, \varepsilon)$, is obtained for each fixed energy on a symmetric momentum grid with 60 p (p') points and 40 x points. Because the momentum region that contributes to a solution of the two-body t matrix is quite different from the region of importance in a three-body calculation, we map our solution for t_s onto the momentum grid relevant for the three-body transition amplitude. We do this by applying the Lippmann-Schwinger equation repeatedly. The t matrix $t_s(p', p, x, \varepsilon)$ is obtained at energies $\varepsilon = E - (3/4m)q^2$, exactly at the q values needed in the three-body transition amplitude of Eq. (2.19).

In carrying out our calculations, it turns out that there are essentially two separate issues governing the quality of the results. The first is the angle dependence of the transition amplitude of Eq. (2.19). It is to be expected that the angle dependence is weak at low energies and increases with higher energies, reflecting the need to include more and more partial waves at higher energies in partial-wave-based calculations. As example we list in Table I the elastic and breakup total cross sections together with the total cross section extracted from the imaginary part of U in the forward direction, Eq. (3.23). At 0.01 GeV, 12 points for all angles are clearly sufficient, whereas at 0.1 GeV this is not so. Table I lists the elastic, breakup, and total cross sections as functions of the angle variables, and we see that one needs at least 16 points for all angles. At 0.5 GeV

we find that the biggest angular dependence occurs in x_q and x'' and the least dependence in the azimuthal angle φ'' and the angle $x_{pq}^{q_0}$, and we take this into account in our choice of angle points.

The other issue is the quality of the calculation in the singular regime, i.e., in the integration region bounded by q_{\max} in Fig. 2. We divide the integration grid for q'' into the intervals $(0, q_{\max}) \cup (q_{\max}, \bar{q})$, where $q_{\max} = \sqrt{(4m/3)E}$ and $\bar{q} = 20 \text{ fm}^{-1}$. The interval boundaries 0 and q_{\max} are handled explicitly. As the energy increases, q_{\max} increases, and we need to take this into account by changing the distribution of the q'' points as functions of energy within the different q'' intervals, i.e., put more points into the interval $(0, q_{\max})$ and less into (q_{\max}, \bar{q}) . From the number of points in $(0, q_{\max})$, one can define an average point distance $\Delta_q \equiv q_{\max}/[\text{number of points in}(0, q_{\max})]$ in this interval. In Fig. 3 we show the dependence of the calculation on Δ_q by using the percentage error $\delta_{\text{opt}} = |\sigma_{\text{opt}} - \sigma_{\text{el}} - \sigma_{\text{br}}|/\sigma_{\text{opt}} \times 100$ in the fulfillment of the optical theorem as a quality measure. At 0.01 GeV it is quite easy to make the average point distance very small in the interval $(0, q_{\max})$, because q_{\max} is only 75 MeV. The top panel of Fig. 3 shows that the percentage error δ_{opt} drops linearly below 0.1% and flattens out at $\Delta_q = 3.5 \text{ MeV}$, where the most likely errors in the interpolation start to play a role. At projectile energy 0.1 GeV, q_{\max} is already 284 MeV and Δ_q is naturally much larger with a reasonable number of q'' points. The dependence of the δ_{opt} for 0.1 GeV on Δ_q is shown in the middle panel of Fig. 3 for two different cases. An angular grid size of 12 points is indicated by the open squares, one of 24 points by crosses. A comparison of the calculations shows that, at $\Delta_q = 15 \text{ MeV}$, the calculation with 12 angular points cannot be improved any further; the calculations start to oscillate for smaller Δ_q , accidentally giving very good agreement at $\Delta_q = 13 \text{ MeV}$. Increasing the number of angle points to 24 shows a further linear decrease in the error (cross symbols)

TABLE I. The total elastic and breakup cross sections together with the total cross section extracted by means of the optical theorem calculated from a Malfliet-Tjon-type potential at two selected energies (0.01 and 0.5 GeV) as functions of the grid points. The double-prime quantities are the integration variables. The calculations are carried out in the coordinate system in which q_0 is aligned parallel to the z axis.

$E_{\text{lab}}(\text{GeV})$	p	x_p	$x_{pq}^{q_0}$	x_q	q, q''	x''	φ''	$\sigma_{\text{opt}}(\text{mb})$	$\sigma_{\text{el}}(\text{mb})$	$\sigma_{\text{br}}(\text{mb})$	$\sigma_{\text{el}} + \sigma_{\text{br}}(\text{mb})$
0.01	49	4	4	4	49	4	4	1913.48	1799.08	67.81	1866.89
	49	8	8	8	49	8	8	1886.84	1807.50	70.14	1877.64
	49	12	12	12	49	12	12	1904.99	1820.77	73.75	1894.52
	49	16	16	16	49	16	16	1903.22	1820.46	73.20	1893.66
0.1	49	12	12	12	49	12	12	335.57	259.95	83.10	343.05
	49	16	16	16	49	16	16	343.17	265.83	75.84	341.67
	49	23	23	16	49	16	20	344.34	270.05	76.23	346.28
	49	23	23	24	49	24	20	346.16	272.04	76.55	348.59
0.5	49	12	12	12	49	12	12	40.17	12.05	66.32	78.37
	49	16	16	16	49	16	16	65.62	47.76	32.73	80.49
	49	20	20	16	49	16	20	65.93	47.61	38.16	86.22
	49	20	16	20	49	20	16	85.19	61.16	28.84	90.00
	49	20	20	20	49	20	20	85.71	61.30	29.86	91.19
	49	24	20	20	49	20	20	85.72	61.24	30.56	91.80
	49	20	20	24	49	24	20	102.17	64.96	33.74	98.70
	49	23	23	24	49	24	20	110.35	64.28	36.42	100.70

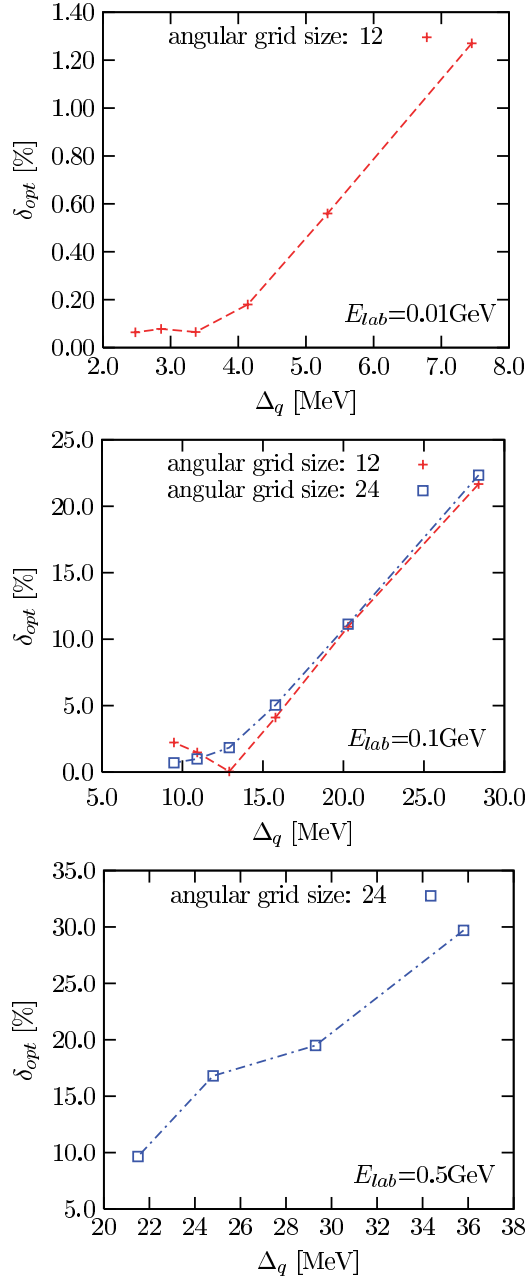


FIG. 3. (Color online) The percentage of error in the optical theorem as a function of the average distance Δ_q of the integration grid points q'' in the interval $(0, q_{\max})$ at the selected laboratory projectile energies $E_{\text{lab}} = 0.01$ GeV (top panel), $E_{\text{lab}} = 0.1$ GeV (middle panel), and $E_{\text{lab}} = 0.5$ GeV (bottom panel).

into the 1% region of δ_{opt} at $\Delta_q = 9$ MeV. This is consistent with the findings shown in the top panel. We continue to study the dependence of Δ_q at 0.5 GeV, where $q_{\max} = 644$ MeV. Here we immediately use 24 angle points, as suggested from Table I. A total of 30 integration points in $(0, q_{\max})$ leads to $\Delta_q = 22$ MeV and $\delta_{\text{opt}} \approx 10\%$, which is consistent with the values in the middle panel. The 10% error is also consistent with the value for the total breakup cross section in the last row of Table I, which indicates that σ_{br} is not yet converged. From the systematics at the different energies shown in

TABLE II. The total elastic cross section total breakup cross section, and total cross section extracted by means of the optical theorem calculated in different coordinate systems at selected energies. The choice of coordinate system, i.e., which vector is aligned parallel to the z axis, is indicated by the superscripts q_0 , q , and p .

E_{lab} (GeV)	$\sigma_{\text{el}}^{q_0}$ (mb)	σ_{el}^q (mb)	$\sigma_{\text{br}}^{q_0}$ (mb)	σ_{br}^q (mb)	σ_{br}^p (mb)	$\sigma_{\text{opt}}^{q_0}$ (mb)	σ_{opt}^q (mb)
0.003	2561.74	2561.14	0.0	0.0	0.0	2562.65	2562.65
0.01	1820.46	1820.51	73.20	73.55	73.13	1903.22	1902.56
0.1	272.04	272.20	76.55	75.18	75.08	346.16	346.16
0.5	64.28	64.61	36.42	36.39	35.55	110.35	110.35
1.0	21.90	21.90	23.44	23.46	23.40	49.59	49.59

Fig. 3 we can extrapolate on the Δ_q needed to reduce the error in the optical theorem. Because of computer time limitations we have not pushed this any further.

In Table I the total elastic, the total breakup, and the total cross section evaluated according to Eq. (3.23) by means of the optical theorem are given and shown as functions of various sets of grid points. The momentum grids for p and q are discretized with 49 points each. The integration variable q'' plays the same role as q and is therefore also discretized with 49 points distributed over the intervals $(0, q_{\max}) \cup (q_{\max}, \bar{q})$ in an energy-dependent way according to the insights described above. The values given in the last row of each energy correspond to the points at the smallest Δ_q in Fig. 3.

A nontrivial test for the quality accuracy of our calculation is the numerical verification of optical theorem Eq. (3.23). Our results are given for selected energies in Table II. Here we show two sets of cross sections, distinguished by the superscripts q_0 and q for the total and the elastic cross sections, respectively. The superscripts indicate that the calculation is carried out by choosing the z axis either parallel to $\hat{\mathbf{q}}_0$ or to $\hat{\mathbf{q}}$. Performing the calculation with two different choices of the z axis is a nontrivial test for our choice of independent variables as well as for the entire calculation. The total breakup cross section is also calculated in a coordinate system in which the z axis is parallel to $\hat{\mathbf{p}}$, indicated by σ_{br}^p . The calculations are based on the largest grids given in Table I and show a very good agreement of the results obtained in the different coordinate systems. This indicates the numerical rotational invariance of our calculations.

On top of convergence tests for the Padé summation, we insert the resulting amplitude \hat{T} again into the integral of Eq. (2.19), leading to a second amplitude \hat{T}' . Both amplitudes should be identical within our numerical errors. We check this by evaluating the cross sections again by using the second amplitude. We document the results in Table III for the differential elastic cross section at selected angles. The table shows excellent agreement of the two values of the cross section.

Finally, another highly nontrivial test of our calculation is the independence of the cross sections from the arbitrary angle φ_{q_0} and the sign of $\sin(\varphi_p - \varphi_{q_0})$. This is documented in Tables IV and V for the energy $E = 3$ MeV. To check the rotational invariance numerically, the calculations are carried

TABLE III. The elastic differential cross sections at different energies for selected scattering angles. The cross section labeled T results from the converged solution of the integral equation, Eq. (2.19). The column labeled T' is calculated by reinserting the original solution into the Faddeev equation with $T' = tP + tG_0PT$. The calculations are based on a Malfliet-Tjon-type potential, as described in the text.

E_{lab} (GeV)	$\theta_{\text{c.m.}}$ (deg)	$\frac{d\sigma_{\text{el}}}{d\Omega_{\text{c.m.}}} _T$ (mb)	$\frac{d\sigma_{\text{el}}}{d\Omega_{\text{c.m.}}} _{T'}$ (mb)
0.01	0.0	537.536	537.536
	21.8	420.036	420.036
	62.1	70.726	70.725
	93.4	38.289	38.289
	151.5	227.899	227.899
0.2	0.0	676.821	676.821
	21.8	148.880	148.880
	62.1	0.363	0.363
	93.4	0.223	0.223
	151.5	0.010	0.010
0.5	0.0	519.389	519.389
	21.8	16.209	16.209
	26.3	4.430	4.430
	62.1	0.088	0.088
	93.4	0.005	0.005
	151.5	0.004	0.004
1.0	0.0	$3.903 \times 10^{+2}$	$3.903 \times 10^{+2}$
	21.8	5.325×10^{-1}	5.325×10^{-1}
	62.1	4.072×10^{-4}	4.072×10^{-4}
	93.4	2.678×10^{-3}	2.678×10^{-3}
	151.5	3.705×10^{-4}	3.703×10^{-4}

out in two different coordinate systems, one in which q_0 is parallel the z axis, and one in which \mathbf{q} is parallel to z . Both tables show excellent agreement for the cross sections, and thus we conclude that our choice of variables is correct.

V. SCATTERING CALCULATIONS AT INTERMEDIATE ENERGIES

Although we neglect spin and isospin degrees of freedom and stay in a strictly nonrelativistic framework, we nevertheless can provide first qualitative insights for various cross sections in three-body scattering in the intermediate-energy regime, which we define as being from 200-MeV to 1-GeV projectile energy. The focus of our investigations is the

TABLE IV. The total elastic cross sections at $E_{\text{lab}} = 3.0$ MeV calculated for different values of the angle φ_{q_0} with the $+$ sign of $\sin(\varphi_p - \varphi_{q_0})$. The calculations are carried out in two different coordinate systems, characterized by the superscripts q_0 and q , which indicate which vector is chosen to be parallel to the z axis.

φ_{q_0} (rad)	$\sigma_{\text{el}}^{q_0}$ (mb)	σ_{el}^q (mb)	$\sigma_{\text{opt}}^{q_0}$ (mb)	σ_{opt}^q (mb)
0.0	2561.736	2561.138	2562.649	2562.649
$\frac{\pi}{2}$	2560.885	2560.729	2562.496	2562.496
π	2561.550	2561.206	2562.091	2562.091

TABLE V. The total elastic cross sections at $E_{\text{lab}} = 3.0$ MeV calculated for different signs of $\sin(\varphi_p - \varphi_{q_0})$, where $\varphi_{q_0} = 0$. The meaning of the superscripts is the same as in Table IV.

sign [$\sin(\varphi_p - \varphi_{q_0})$]	$\sigma_{\text{el}}^{q_0}$ (mb)	σ_{el}^q (mb)	$\sigma_{\text{opt}}^{q_0}$ (mb)	σ_{opt}^q (mb)
+	2561.736	2561.138	2562.649	2562.649
-	2559.674	2559.536	2560.091	2560.091

question of which orders of rescattering in the two-body t matrix are needed to come close to the exact result, namely the solution of the Faddeev equation.

As a model two-body interaction we choose a superposition of two Yukawa interactions of the Malfliet-Tjon type [25]:

$$V(\mathbf{p}', \mathbf{p}) = \frac{1}{2\pi^2} \left[\frac{V_R}{(\mathbf{p}' - \mathbf{p})^2 + \mu_R^2} - \frac{V_A}{(\mathbf{p}' - \mathbf{p})^2 + \mu_A^2} \right]. \quad (5.1)$$

The parameters are given in Table VI and fitted such that the potential supports a two-body bound state, the “deuteron,” at -2.23 MeV. As the first result, we show in Fig. 4 the total cross section together with the total elastic and total breakup cross sections as functions of the laboratory projectile energy. In addition, the total cross section is also evaluated by means of the optical theorem as a test of our numerics. This duplicates the information already given in Table III. We see that the optical theorem is quite well fulfilled. The figure shows that at roughly 1 GeV the total elastic and total breakup cross sections become equal in magnitude in our model.

Next we show in Fig. 5 the angular distribution in elastic scattering for a set of selected energies. In addition to the exact Faddeev result, the cross sections are evaluated in first order in the two-body t matrix, second order in t , third order in t , and fourth order in t , and displayed. First we note that, with increasing energy, the cross section in the forward direction decreases. Furthermore, for all energies shown, the first rescattering (second order in t) always increases the cross section, and subsequent rescatterings lower it again. As expected, for the lowest energy, 0.2 GeV, rescattering terms of higher order are important, and even the fourth order is not yet close to the full result. The same is true for 0.8 GeV. We note that, even at 1 GeV, two rescattering terms (third order in t) are necessary for coming into the vicinity of the final result. The same is true for 0.5 GeV.

In view of the standard “ t - ρ ” impulse approximation for the optical potential in nucleon-nucleus scattering employed at intermediate energies [26], it is interesting to note that the first-order result in t in our model study is quite insufficient. Even at energies larger than 0.5 GeV, rescattering corrections up to the third order are required for coming close to the exact

TABLE VI. The parameters and deuteron binding energy for the Malfliet-Tjon type potential of our calculation. As a conversion factor We use units such that $\hbar c = 197.3286$ MeV fm = 1.

V_A [MeV fm]	μ_A [fm $^{-1}$]	V_R (MeV fm)	μ_R [fm $^{-1}$]	E_d [MeV]
-626.8932	1.550	1438.7228	3.11	-2.2307

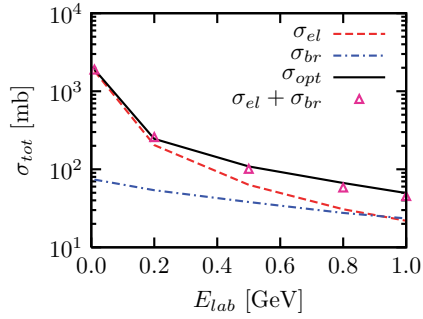


FIG. 4. (Color online) The total elastic cross section σ_{el} (dashed line), the total breakup cross section σ_{br} (dash-dotted line), and the total cross section evaluated by the optical theorem σ_{opt} (solid line) given as functions of the projectile laboratory energy. At the selected energies in which the calculations have been carried out, the sum of the calculated total elastic and breakup cross section, $\sigma_{tot} = \sigma_{el} + \sigma_{br}$, is indicated by the open diamond. The open diamonds coincide with the solid line according to the optical theorem, (Eq. (3.23)), and the numerical values are given in Table II.

result for small scattering angles. Therefore it seems to be likely that the first-order impulse approximation in nucleon-nucleus scattering is insufficient.

In the case of inelastic processes we first regard the semiexclusive reaction $d(N, N')$ in which only one nucleon is detected. We choose three different laboratory energies, 200 MeV, 500 MeV, and 1 GeV and show the inclusive cross section as a few selected angles for the detected nucleon. The results are shown in Figs. 6–10.

At 0.2 GeV the semiexclusive cross section is given in Fig. 6 for the emission angle 24° and in Fig. 7 for the emission angle 39° . Both figures show in the upper panel the entire energy range of the emitted particle. Because the cross section varies by two orders of magnitude, we display it in a logarithmic scale. To better flesh out the peak structures,

the two lower panels show the high and low energies of the emitted particle in a linear scale. Together with the full solution of the Faddeev equation (solid curves), the sums of the lowest orders of the multiple-scattering series are indicated in the figure. The peak at the highest energy of the emitted particle is the so-called final-state interaction (FSI) peak, which develops only when rescattering terms are taken into account. This peak is a general feature of semiexclusive scattering and is present for all energies. The next peak is the quasi-free-scattering (QFS) peak, and one sees that at both angles one needs at least rescattering of fourth order to come close to the full result. However, in contrast to the smaller angle, at the larger angle, 39° in Fig. 7, the first-order result for the larger energies is surprisingly close to the full solution, though the multiple-scattering series is by no means converged, as the following higher orders indicate. We also observe that the QFS peak moves to lower energies of the emitted particle with increasing emission angle. At both angles the very low energies of the emitted particle exhibit a strong peak in first order, which is considerably lowered by the first rescattering. Here the calculation up to third order in the multiple-scattering series seems already sufficient.

For 0.5-GeV incident energy the semiexclusive cross section is given in Fig. 8 for the emission angle 24° and in Fig. 9 for the emission angle 36° . We again see three peaks along the energy axis of the detected nucleon, the FSI and QFS peaks as well as the peak at the extreme low energy of the emitted particle. Again we see that the results based on first and second order in t alone are quite insufficient and higher-order rescatterings cannot be neglected. It is also interesting to observe that, at 24° , Fig. 8, the third- and higher-order rescattering terms shift the peak to higher energies, whereas at the larger angle of 36° the peak positions of the various orders coincide more or less and agree with the peak position of the full calculation. Again, for the peak for the very low energies of the emitted particle, the third-order calculation agrees already quite well with the full result.

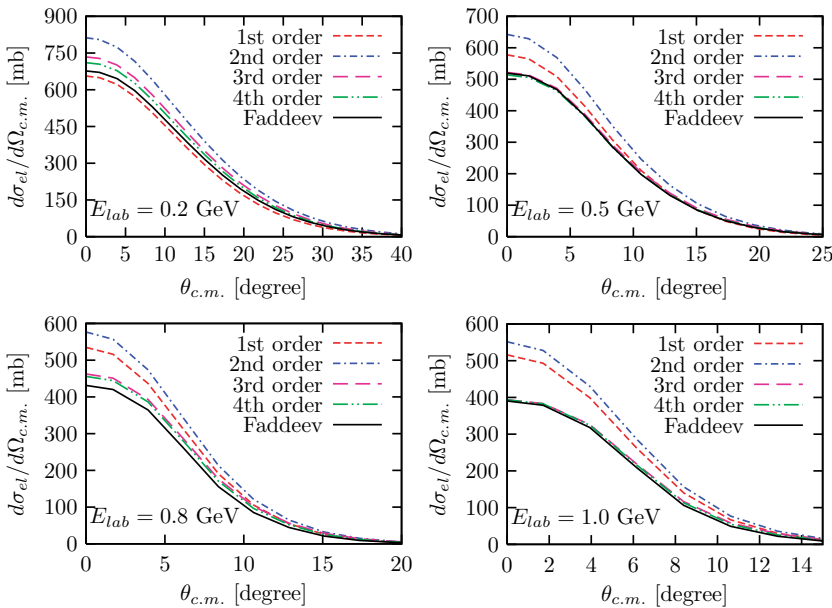


FIG. 5. (Color online) The elastic differential cross sections at 0.2-, 0.5-, 0.8-, and 1.0-GeV projectile energies as functions of the laboratory scattering angle. In all cases the solid curves represent the full solution of the Faddeev equation. The other curves represent the successive sum of different orders in the multiple-scattering series: the short-dashed curves represent the first-order; the dash-dotted curves add up to the second order; the long-dashed curves to the third-order; and the dash-dot-dotted curves to the fourth-order contribution.

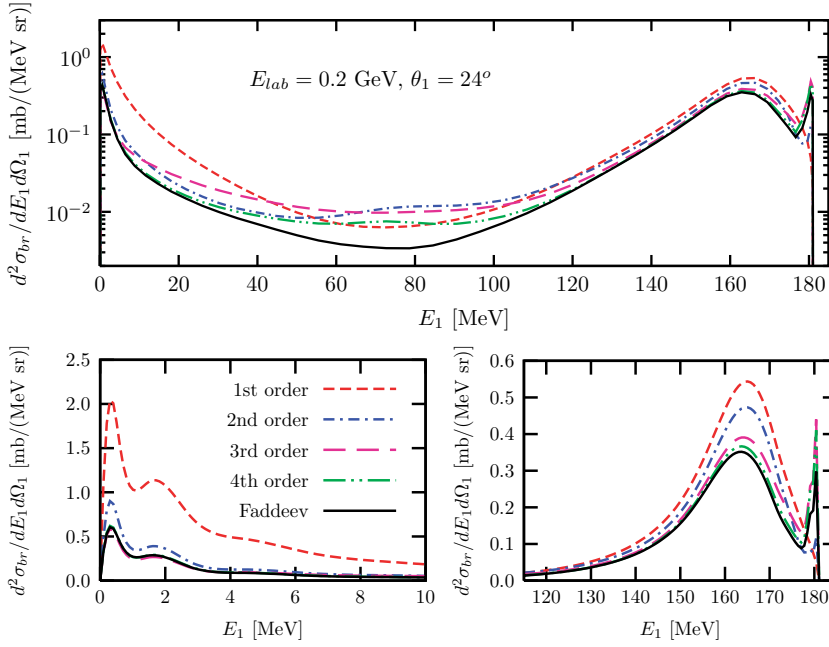


FIG. 6. (Color online) The semiexclusive cross section at 0.2-GeV laboratory incident energy and at 24° emission angle of the emitted particle. The upper panel displays the entire energy range of the emitted particle, whereas the two lower panels show only the low and high energies in a linear scale. The full solution of the Faddeev equation is given by the solid curves in all panels. The contribution of the lowest orders of the multiple-scattering series added up successively is given by the other curves, as indicated in the legend of the lower left-hand panel.

At 1 GeV the situation is similar. As examples we have selected two angles: 18°, displayed in Fig. 10, and 30°, displayed in Fig. 11. For the small emission angle the second rescattering shifts the QFS peak toward higher energies; at the larger angle this is not the case. Our studies indicate that this is a general phenomenon occurring at all energies under consideration. There exists a critical maximum energy E_1^{\max} of the emitted particle, corresponding to a specific emission angle, at which such a shift in the QFS peak through higher-order rescattering

terms can occur. At 0.5-GeV projectile energy this maximum energy is 0.44 GeV; at 1 GeV it is 0.88 GeV. If one considers the ratio (E_1^{\max}/E_{lab}) , then one finds for both cases that, if this ratio is larger than 0.8, the QFS peak is shifted by higher-order rescattering terms. This could be interpreted as an interference between the QFS and the FSI mechanisms. If this ratio is smaller than 0.8, then the FSI peak is small and higher orders in the multiple-scattering series do not change the position of the QFS peak. In addition, it seems that at the

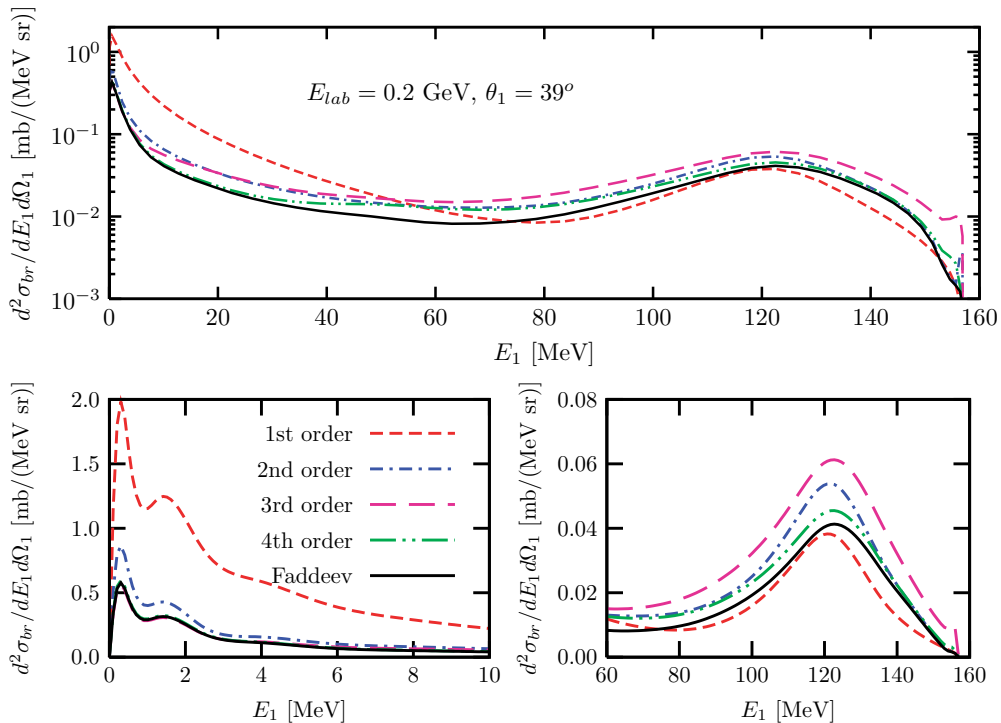


FIG. 7. (Color online) Same as Fig. 6 but for an angle of 39° of the emitted particle.

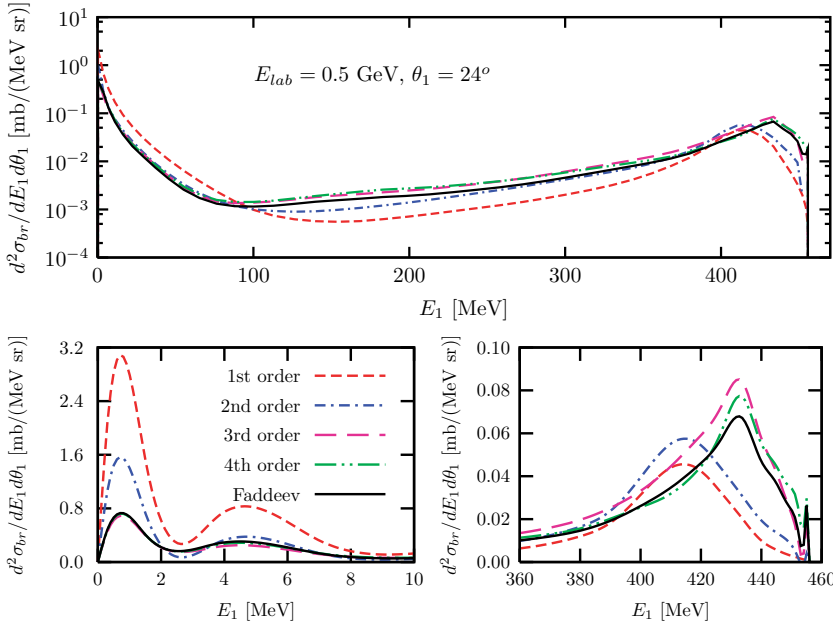


FIG. 8. (Color online) The semi-exclusive cross section at 0.5-GeV laboratory incident energy and at 24° angle of the emitted particle. The upper panel displays the entire energy range of the emitted particle, whereas the two lower panels show only the low and high energies in a linear scale. The full solution of the Faddeev equation is given by the solid curves in all panels. The contribution of the lowest orders of the multiple-scattering series added up successively is given by the other curves, as indicated in the legend of the lower left-hand panel.

larger angle (Fig. 11) the multiple-scattering series converges a little faster with respect to the higher orders compared with the smaller angle (Fig. 10). The final result for the peak at the very low energy of the emitted particle is, as before, reached with two rescattering contributions. It is remarkable that for the energies between about 200 and 500 MeV of the emitted particle the first rescattering contributes almost an order of magnitude to the cross section.

We can make a first contact to calculations based on realistic nucleon-nucleon (*NN*) forces. In Ref. [17] the semiexclusive process *d*(*p*, *n*) has been determined in first order in *t* based on the *NN* potentials AV18 [27] and Bonn-B [28]. In the upper panel of Fig. 12 we compare our first-order calculation at 495-MeV projectile laboratory energy and 18° emission angle with the first-order calculations from Ref. [17] based on the

two realistic potentials. The position of the peak is determined only through kinematics; thus the peak position coincides for all three calculations. Although our model calculation refers to bosons and the potential contains only the crude features of a central short-range repulsion and intermediate-range attraction, the magnitudes of the cross sections differ only by roughly 20%. In the lower panel we show the contributions of the first orders of the multiple-scattering series successively summed together with the exact solution of the Faddeev equation for our model. At this angle and energy the contribution of the first rescattering (second-order in the multiple-scattering series) is quite weak; the contributions of the next two orders are large and lower the size of the peak. At very high energies of the emitted particle, the fourth order in the multiple-scattering series is still not yet close to the exact

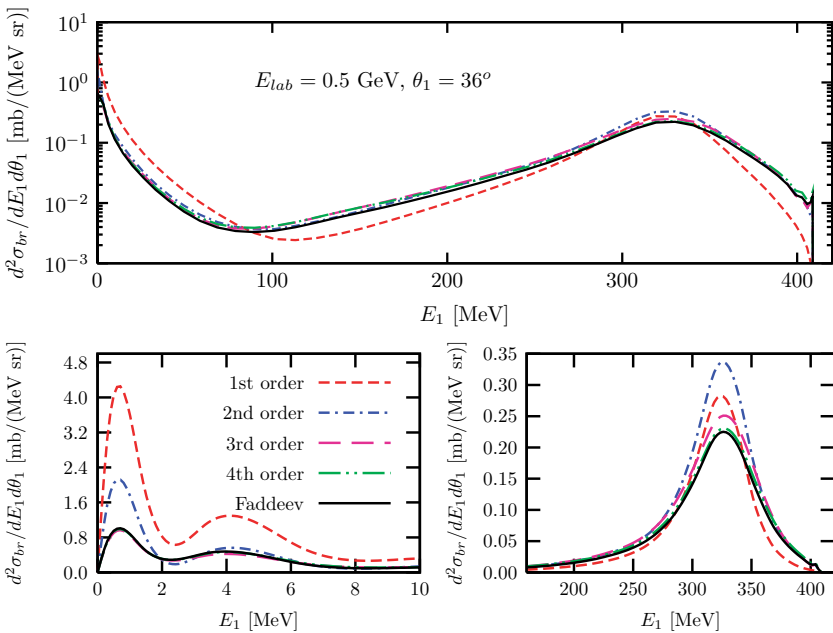


FIG. 9. (Color online) Same as Fig. 8 but for an angle of 36° of the emitted particle.

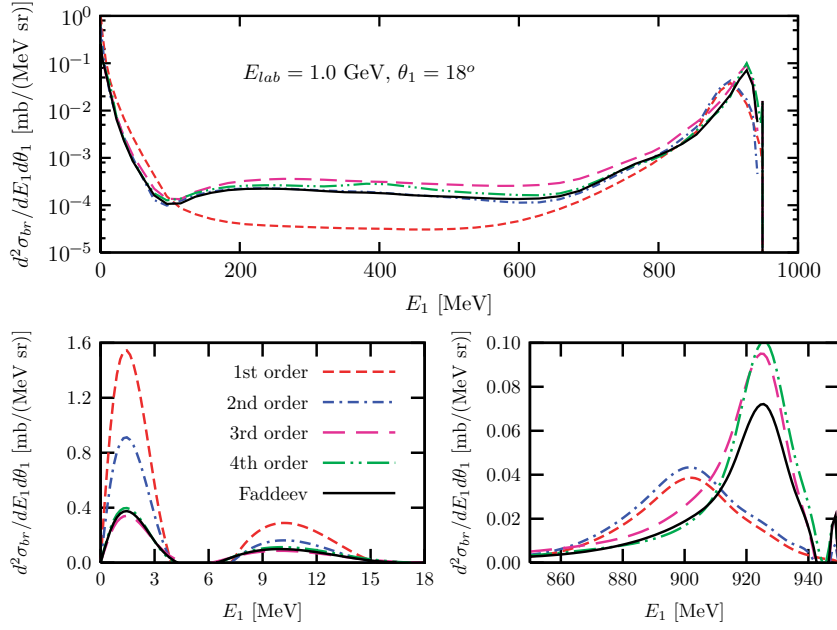


FIG. 10. (Color online) The semiexclusive cross section at 1-GeV laboratory incident energy and at 18° angle of the emitted particle. The upper panel displays the entire energy range of the emitted particle, whereas the two lower panels show only the low and high energies in a linear scale. The full solution of the Faddeev equation is given by the solid curves in all panels. The contribution of the lowest orders of the multiple-scattering series added up successively is given by the other curves, as indicated in the legend of the lower left-hand panel.

result. Therefore we conjecture that at this energy calculations with realistic forces will also require higher-order rescattering contributions.

Finally we comment on a recently measured and analyzed reaction $pd \rightarrow (pp)n$ at high momentum transfer [29,30]. In this experiment the breakup configuration has been chosen such that the neutron is ejected at extreme backward angles and the two protons at extreme forward angles. The measurement was carried out at giga-electron-volt laboratory energies. The

experimental data [29] were analyzed in Ref. [30] with first- and second-order processes in the NN t matrix, including a Δ -isobar mechanism. Within our nonrelativistic toy model for three bosons, we are of course unable to analyze the data. However, within our model we can give a clear answer as to whether higher-order rescattering processes are essential in this reaction. In Refs. [29,30] the data are integrated over a small interval of the relative pp energy between 0 and 3 MeV and averaged over the neutron c.m. angle in the interval

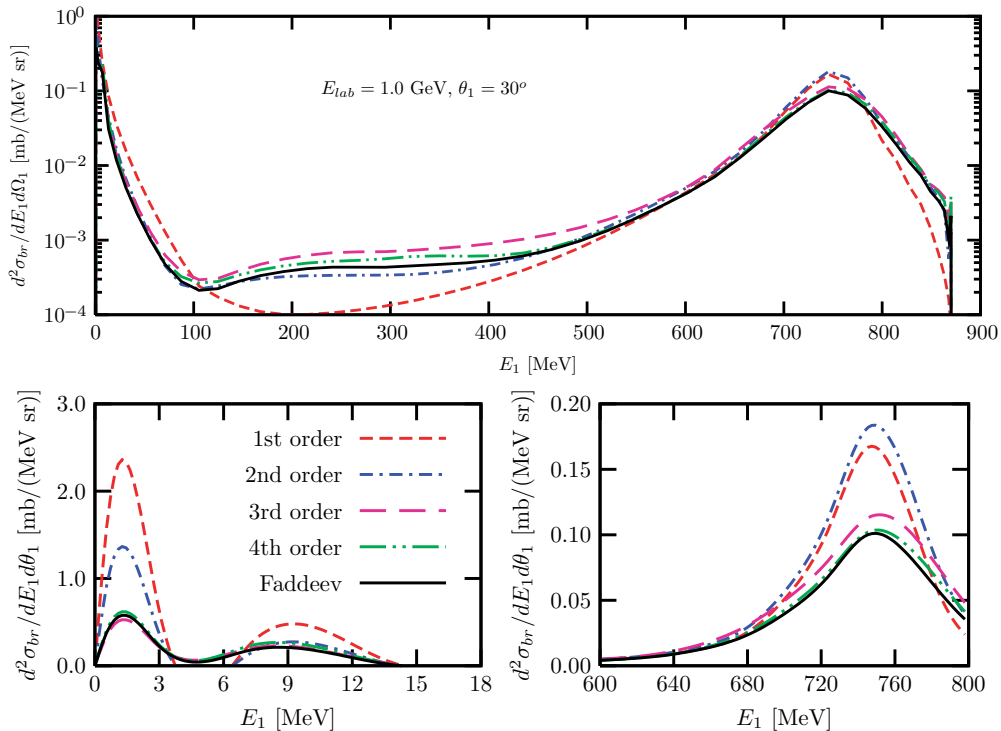


FIG. 11. (Color online) Same as Fig. 10 but for an angle of 30° of the emitted particle.

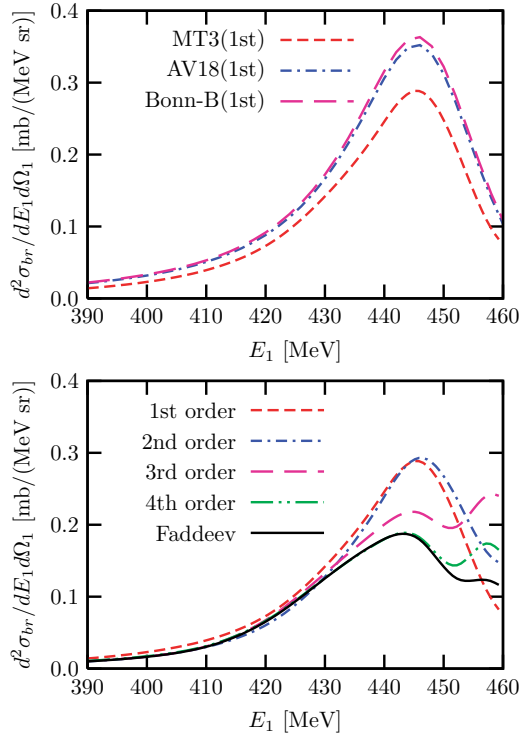


FIG. 12. (Color online) The semiexclusive cross section at 495-MeV laboratory incident energy and at 18° angle of the emitted particle. The upper panel displays the first-order results obtained from the realistic potentials AV18 [27] (long-dashed curve) and Bonn-B [28] (dashed-dotted curve) together with our calculation based on the scalar Malfliet-Tjon potential of Eq. (5.2) (dashed curve). The lower panel displays again our first-order calculation from the upper panel (dashed curve), together with a successive addition of the next three rescattering terms. The exact solution of the Faddeev equation is given by the solid curve.

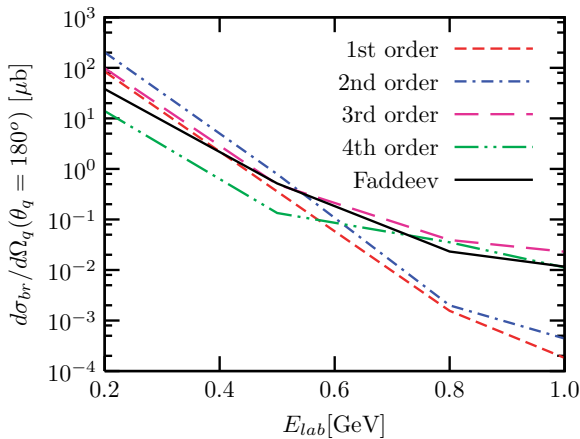


FIG. 13. (Color online) The cross section (c.m.) for the semiexclusive breakup reaction in which two particles emerge in the forward direction with a relative energy between 0 and 3 MeV, and one particle is detected at a backward angle as a function of the projectile laboratory energy. The result of the full Faddeev calculation is given by the solid curve and is compared with calculations based on the lowest orders of the multiple-scattering series in t added up successively, as indicated in the legend.

between 172° and 180° . In our qualitative study we fix the c.m. angle of one particle at 180° , but integrate over the relative energy $E_{pp} = p^2/m$ of the two other particles between 0 and 3 MeV. Thus, we evaluate the cross section as

$$\frac{d\sigma}{d\Omega_q} = (2\pi)^4 \left(\frac{2}{3}\right)^2 \frac{m^2}{q_0} \int_0^{\sqrt{mE_{pp}}} dp p^2 q \times \int d\hat{p} |U_0(p, x_p, x_{pq}^{q_0}, x_q = -1, q, q_0)|^2. \quad (5.2)$$

Because we choose the z axis parallel to $\hat{\mathbf{q}}_0$, and $\hat{\mathbf{q}}$ is antiparallel to $\hat{\mathbf{q}}_0$, the φ_p dependence is directly given by $x_{pq}^{q_0} = \cos \varphi_p$. Our calculations are carried out for projectile laboratory energies between 0.2 and 1 GeV and are displayed in Fig. 13. Here we compare different low orders in the two-body t matrix with the full solution of the Faddeev equation. We note that all our calculations exhibit a smooth falloff as a function of the projectile energy. This behavior is present in the data of Ref. [29]. None of our calculations shows a dip structure around 0.7 GeV as indicated for some of the calculations in Ref. [30]. The reason may be that our calculation is carried out in three dimension, i.e., all partial waves are included exactly, whereas in Ref. [30] only the lowest partial waves are considered. At low projectile energies, rescattering terms of higher order still give considerable contributions to the cross section. At 1 GeV the first-order calculation is an order of magnitude smaller than the result of the full calculation. It is interesting to note that at 1 GeV the contribution from the first rescattering is relatively small, and one needs to go to the third order in t to come close to the full result for this particular breakup configuration.

In addition to the specific breakup configuration described above, a measurement of the extreme backward-scattering elastic pd cross section has been investigated in Ref. [30]. Instead of a forward-scattered pp pair with very small relative energy, one now has a forward-going deuteron. This situation corresponds to elastic scattering from a deuteron at a backward

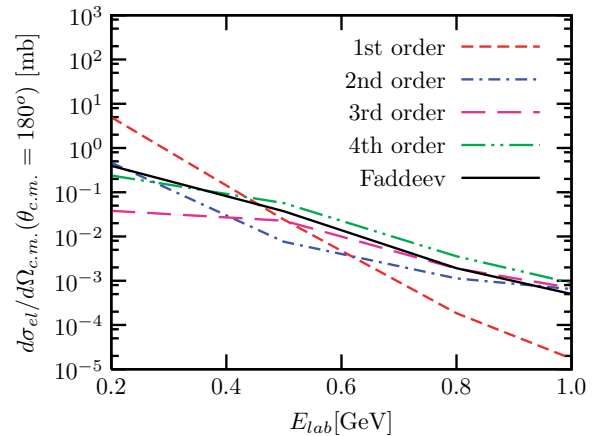


FIG. 14. (Color online) The elastic cross section (c.m.) at a backward angle as a function of the projectile laboratory energy. The result of the full Faddeev calculation is given by the solid curve and is compared with calculations based on the lowest orders of the multiple-scattering series in t added up successively, as indicated in the legend.

angle. To investigate the influence of rescattering for this reaction we plot in Fig. 14 the backward angle of the elastic cross section at energies from 0.2 to 1 GeV and compare the result of the full Faddeev calculation with calculations based on low orders in the multiple-scattering series. The figure shows that the first-order calculation is insufficient over the entire energy regime considered, except of course for the crossing point around 0.5 GeV. The first rescattering contribution (second-order calculation), though close at 0.2 GeV, is insufficient below roughly 0.9 GeV. The figure also shows that at about 0.9 GeV the relative magnitude of contributions from the second- and higher-order rescattering become small. Thus we conclude that at 1 GeV one needs at least one rescattering to be in the vicinity of the full result for the elastic cross section at the backward angle.

VI. SUMMARY AND CONCLUSIONS

In this study we perform fully converged Faddeev calculations for three identical bosons interacting by nonseparable forces in the intermediate-energy range between about 0.2 and 1.0 GeV. To the best of our knowledge these are the first calculations of this kind. The key point is to neglect the partial-wave decomposition generally used at low energies and to work directly with momentum vectors. Thus all partial waves are exactly included. A suitable choice of variables is important. Besides the two magnitudes of the two relative Jacobi momenta \mathbf{p} and \mathbf{q} we choose the angles between the vectors \mathbf{p} and \mathbf{q}_0 and between \mathbf{q} and \mathbf{q}_0 , where \mathbf{q}_0 is the projectile momentum. The fifth variable is the angle between the two planes spanned by \mathbf{p}, \mathbf{q}_0 and \mathbf{q}, \mathbf{q}_0 . In the technical piece of the work we introduce for the first time a spline-based integration of the moving logarithmic singularities, which is a very valuable alternative to procedures used so far. The numerical results are converging, as documented in Sec. III. In Sec. V we show elastic and inelastic (breakup) cross sections in the above-mentioned intermediate-energy range. We focus on the question of how many orders of rescattering beyond the often-used first-order calculation in the two-body t matrix are needed for coming close to the full Faddeev result. We find that in nearly all cases studied processes of at least second- and third-order rescattering are required. Whether this will be also required in performing calculations with realistic dynamical inputs has to be examined in the future.

In one case we can make first contact to a result based on the NN forces AV18 and Bonn-B, which are considered to be realistic in the sense that they describe all NN data below 350 MeV extremely well. This was the semiexclusive cross section at 495 MeV evaluated in first order in the NN t matrix. Of course, at that energy AV18 and Bonn-B are at the upper limit of their applicability. Despite our simple two-body model force, a superposition of two Yukawa interactions, one attractive, the other repulsive, our results turns out to be within about 20% to the calculation based on the realistic models. This shows that our investigations might allow some conclusions about results based on present and future models with more dynamical inputs.

As a first example for considering data in the light of our toy model we study the extreme backward elastic dN

scattering over the energy range from 0.2 to 1.0 GeV. We find that first-order results in the two-body t matrix are totally insufficient, and it is only around 1 GeV that the first-order rescattering comes close to the full result. Parallel to those data in elastic scattering in Refs. [29,30], the complete breakup process $d(p, n)pp$ has also been investigated. Here the neutron was ejected antiparallel to the beam direction and the two protons at extreme forward angles with a very small relative energy. Again we study the significance of rescattering processes and find that, for this particular breakup configuration, two rescatterings are necessary for getting close to the result of the full Faddeev calculation.

In conclusion we can say that the three-body Faddeev equations can be safely solved at intermediate energies by using directly momentum vectors. Calculations based on partial-wave decomposition would be hardly feasible at these energies.

Further studies scanning the complete three-body phase space for the total breakup are underway. This may be important in order to shed light on previous theoretical analysis of $p(d, ppn)$ reactions that relied on low-order reaction mechanisms.

Based on our current experience it appears that, if low-order rescattering processes will turn out to be sufficient for certain phase-space regions, realistic calculations including spin and isospin will be feasible, even including three-body forces. A first step in evaluating the $d(p, n)pp$ breakup cross section in first order with a currently used two-pion exchange, three-nucleon force model is already underway [31]. What is badly needed now are realistic models for nuclear forces in the intermediate-energy regime we study. This paper allows us to conclude that it will be feasible to extend the calculations to realistic dynamics.

In Ref. [17] the effect of relativistic kinematics was studied in the (p, n) charge exchange reaction on deuterium between 0.1 and 0.5 GeV in a first-order Faddeev calculation. This work concluded that the effects that are due to relativistic kinematics are quite visible at 0.5 GeV, specifically in the location of the position of the QFS peak, which is purely determined by kinematics. Therefore we should expect that the relativistic kinematics will influence our results, especially at energies larger than 0.5 GeV. Of course, there are other dynamical relativistic effects. For energies below ~ 0.25 GeV those relativistic effects were studied in neutron-deuteron elastic scattering in Ref. [32]. There it was found that the combination of relativistic effects consistently incorporated is negligible below 0.1 GeV and manifests itself at 0.25 GeV, mostly at large scattering angles. What happens at the energies we considered when relativistic effects (kinematical and dynamical ones) are incorporated is uncharted territory so far, and we want to refrain from speculation. Work in this direction is, however, underway.

ACKNOWLEDGMENTS

We thank I. Fachruddin for allowing us to use his results for comparison with ours. W. G. thanks K. Miyagawa for fruitful collaboration on the spline-based integration of the logarithmic singularities. This work was performed in part under the auspices of the U.S. Department of Energy under

contract no. DEFG02-93ER40756 with Ohio University. We thank the National Energy Research Supercomputer Center for the use of their facilities.

APPENDIX: THE φ'' INTEGRATION

According to Eqs. (2.19), (2.18), and (2.20), the φ'' integration for fixed $p, q, x_p, x_q, x_{pq}^{q_0}, q'',$ and x'' can be written as

$$I(\varphi_{q_0}, \varphi_p) = \int_0^{2\pi} F[\cos(\varphi'' - \varphi_{q_0})]G[\cos(\varphi'' - \varphi_p)]d\varphi'', \quad (\text{A1})$$

where the F and G are known functions from \hat{t}_s and \hat{T} . The substitution $\varphi' = \varphi'' - \varphi_{q_0}$ leads to

$$\begin{aligned} I(\varphi_{q_0}, \varphi_p) &= \int_0^{2\pi} F[\cos \varphi']G\{\cos[\varphi' - (\varphi_p - \varphi_{q_0})]\}d\varphi' \\ &\equiv I(\varphi_{q_0} - \varphi_p). \end{aligned} \quad (\text{A2})$$

Moreover, splitting this integral as

$$\begin{aligned} I(\varphi_{q_0} - \varphi_p) &= \int_0^{\pi} F[\cos \varphi']G\{\cos[\varphi' - (\varphi_p - \varphi_{q_0})]\}d\varphi' \\ &+ \int_{\pi}^{2\pi} F[\cos \varphi']G\{\cos[\varphi' - (\varphi_p - \varphi_{q_0})]\}d\varphi' \end{aligned} \quad (\text{A3})$$

and substituting $\varphi' = 2\pi - \varphi''$ in the second integral, one obtains

$$\begin{aligned} I(\varphi_p - \varphi_{q_0}) &= \int_0^{\pi} F[\cos \varphi'']G\{\cos[\varphi'' - (\varphi_p - \varphi_{q_0})]\} \\ &+ G\{\cos[\varphi'' + (\varphi_p - \varphi_{q_0})]\}d\varphi'' \\ &\equiv I(|\varphi_p - \varphi_{q_0}|). \end{aligned} \quad (\text{A4})$$

Consequently, the result for the φ integration in Eq. (A2) or Eq. (A4) does not depend on the choice of the sign in $\sin(\varphi_p - \varphi_{q_0}) = \pm\sqrt{1 - \cos^2(\varphi_p - \varphi_{q_0})}$. Only $\cos(\varphi_p - \varphi_{q_0})$ is fixed by Eq. (2.21), and has to be known.

Because the integral I in Eq. (A4) depends on only the difference of the angles $(\varphi_p - \varphi_{q_0})$, one can choose φ_{q_0} arbitrarily, and thus $\sin \varphi_{q_0}$ and $\cos \varphi_{q_0}$ required in Eqs. (2.18). Moreover, the trivial identities

$$\begin{aligned} \cos \varphi_p &= \cos \varphi_{q_0} \cos(\varphi_p - \varphi_{q_0}) - \sin \varphi_{q_0} \sin(\varphi_p - \varphi_{q_0}), \\ \sin \varphi_p &= \sin \varphi_{q_0} \cos(\varphi_p - \varphi_{q_0}) + \cos \varphi_{q_0} \sin(\varphi_p - \varphi_{q_0}), \end{aligned} \quad (\text{A5})$$

are the input for $\cos(\varphi_p - \varphi'')$ needed in Eqs. (2.20). The arbitrary choice of φ_{q_0} is a good check for the numerical correctness of the choice of variables, and we carried out those tests.

-
- [1] J. L. Friar, G. L. Payne, W. Glöckle, D. Hüber, and H. Witala, Phys. Rev. C **51**, 2356 (1995).
- [2] H. Witala, Th. Cornelius, and W. Glöckle, Few-Body Syst. **3**, 123 (1988).
- [3] A. Kievsky, M. Viviani, and S. Rosati, Phys. Rev. C **64**, 024002 (2001).
- [4] M. Viviani, A. Kievsky, and S. Rosati, Few-Body Syst. **30**, 39 (2001).
- [5] W. Glöckle *et al.*, Phys. Rep. **274**, 107 (1996).
- [6] W. Glöckle in *Scattering*, Vol. 1, edited by R. Pike and P. Sabatier (Academic Press, New York, 2002), pp. 1339–1359.
- [7] J. Kuros-Zolnierczuk, H. Witala, J. Golak, H. Kamada, A. Nogga, R. Skibinski, and W. Glöckle, Phys. Rev. C **66**, 024004 (2002).
- [8] H. Witala, W. Glöckle, J. Golak, A. Nogga, H. Kamada, R. Skibinski, and J. Kuros-Zolnierczuk, Phys. Rev. C **63**, 024007 (2001).
- [9] K. Chmielewski, A. Deltuva, A. C. Fonseca, S. Nemoto, and P. U. Sauer, Phys. Rev. C **67**, 014002 (2003).
- [10] A. Arriaga, V. R. Pandharipande, and R. B. Wiringa, Phys. Rev. C **52**, 2362 (1995).
- [11] J. Carlson, Phys. Rev. C **36**, 2026 (1987).
- [12] J. Carlson, Phys. Rev. C **38**, 1879 (1988).
- [13] J. G. Zabolitzky, K. E. Schmidt, and M. H. Kalos, Phys. Rev. C **25**, R1111 (1982).
- [14] J. Carlson and R. Schiavilla, Rev. Mod. Phys. **70**, 743 (1998).
- [15] Ch. Elster, W. Schadow, A. Nogga, and W. Glöckle, Few-Body Syst. **27**, 83 (1999).
- [16] H. Liu, Ch. Elster, and W. Glöckle, Few-Body Syst. **33**, 241 (2003).
- [17] I. Fachruddin, Ch. Elster, and W. Glöckle, Phys. Rev. C **68**, 054003 (2003).
- [18] W. Glöckle, *The Quantum Mechanical Few-Body Problem* (Springer-Verlag, Berlin/Heidelberg, 1983).
- [19] W. Schadow, Ch. Elster, and W. Glöckle, Few-Body Syst. **28**, 15 (2000).
- [20] Ch. Elster, J. H. Thomas, and W. Glöckle, Few-Body Syst. **24**, 55 (1998).
- [21] G. A. Baker and J. L. Gammel, eds., *The Padé Approximation in Theoretical Physics* (Academic, New York, 1970).
- [22] D. Hüber, Ph.D. thesis, Bochum University, Bochum, Germany, 1996.
- [23] D. Hüber, H. Witala, A. Nogga, W. Glöckle, and H. Kamada, Few-Body Syst. **22**, 107 (1997).
- [24] H. Liu, Ph.D. dissertation, Ohio University, August 2005.
- [25] R. A. Malfliet and A. J. Tjon, Nucl. Phys. **A127**, 161 (1969).
- [26] L. Ray and G. W. Hoffmann, Phys. Rev. C **31**, 538 (1985); R. Crespo, R. C. Johnson, and J. A. Tostevin, *ibid.* **44**, 1735(R) (1991); Ch. Elster, T. Cheon, E. F. Redish, and P. C. Tandy, *ibid.* **41**, 814 (1990).
- [27] R. B. Wiringa, V. G. J. Stoks, and R. Schiavilla, Phys. Rev. C **51**, 38 (1995).
- [28] R. Machleidt, Adv. Nucl. Phys. **19**, 189 (1989).
- [29] V. Komarov *et al.*, Phys. Lett. **B553**, 179 (2003).
- [30] J. Haidenbauer and Y. N. Uzikov, Phys. Lett. **B562**, 227 (2003).
- [31] I. Fachruddin, private communication.
- [32] H. Witala, J. Golak, W. Glöckle, and H. Kamada, Phys. Rev. C **71**, 054001 (2005).